Journal of Fluorescence
https://doi.org/10.1007/s10895-024-03843-1

REVIEW

Mechanistic Innovations in Fluorescent Chemosensors for Detecting Toxic Ions: PET, ICT, ESIPT, FRET and AIE Approaches

Duraisamy Udhayakumari[1]

Received: 29 May 2024 / Accepted: 3 July 2024

Abstract
Fluorescent chemosensors have become vital tools for detecting toxic ions due to their exceptional sensitivity, selectivity, and rapid response times. These sensors function through various mechanisms, each providing unique advantages for specific applications. This review offers a comprehensive overview of the mechanistic innovations in fluorescent chemosensors, emphasizing five key approaches: Photoinduced Electron Transfer (PET), Fluorescence Resonance Energy Transfer (FRET), Intramolecular Charge Transfer (ICT), Aggregation-Induced Emission (AIE), and Excited-State Intramolecular Proton Transfer (ESIPT). We highlight the substantial progress made in developing these chemosensors, discussing their design principles, sensing mechanisms, and practical applications, with a particular focus on their use in detecting toxic ions relevant to environmental and biological contexts.

Keywords Fluorescence · Fluorophores · Mechanisms · Toxic analytes · Sensing · Detection

Introduction

The detection of toxic ions is a critical task in environmental monitoring, industrial processes, and biomedical diagnostics. Toxic ions, such as heavy metals and harmful anions, pose significant threats to human health and ecosystems [1–3]. Traditional methods for detecting these ions, such as atomic absorption spectroscopy and inductively coupled plasma mass spectrometry, although highly sensitive and specific, are often limited by their complexity, high cost, and the need for extensive sample preparation. Consequently, there is a growing demand for more practical, efficient, and cost-effective detection methods. Fluorescent chemosensors have emerged as promising alternatives due to their high sensitivity, selectivity, rapid response times, and ease of use. These sensors operate by converting the presence of a target ion into a measurable fluorescence signal, enabling real-time and in-situ analysis. The versatility of fluorescent chemosensors is largely attributed to the diverse mechanisms by which they can interact with target ions, each offering distinct advantages tailored to specific detection requirements [4, 5].

This review delves into the mechanistic innovations underpinning the development of fluorescent chemosensors, focusing on five major approaches: Photoinduced Electron Transfer (PET), Fluorescence Resonance Energy Transfer (FRET), Intramolecular Charge Transfer (ICT), Aggregation-Induced Emission (AIE), and Excited-State Intramolecular Proton Transfer (ESIPT). Understanding these mechanisms is crucial for designing effective chemosensors, as each mechanism influences the sensor's performance characteristics, including sensitivity, selectivity, and operational conditions. In this review, we aim to provide a thorough analysis of these five mechanistic approaches, highlighting the design principles, operational mechanisms, and practical applications of fluorescent chemosensors (Table 1). We explore the recent advancements and innovations in detecting toxic ions that are important for the environment and biology, and we discuss future directions and potential challenges in this field [6–10].

Phenomena of fluorescence

Fluorescence is a photophysical phenomenon where a substance absorbs photons, usually in the ultraviolet or visible spectrum, and subsequently re-emits photons at a longer

✉ Duraisamy Udhayakumari
udhaya.nit89@gmail.com;
udayakumari.d@rajalakshmi.edu.in

[1] Department of Chemistry, Rajalakshmi Engineering College, Chennai 602105, India

Published online: 17 July 2024

wavelength. This process involves several key steps such as excitation, vibrational relaxation, internal conversion and fluorescence emission. Fluorescence lifetimes, typically ranging from nanoseconds to microseconds, and quantum yields, which measure the efficiency of fluorescence, are crucial parameters. Fluorescence spectroscopy and microscopy exploit these properties for diverse applications, including biological imaging, where fluorophores tag specific biomolecules, and materials science, where fluorescence signals indicate specific structural or compositional information. Environmental factors such as solvent polarity, temperature, and pH can significantly influence fluorescence intensity and spectra [11, 12], making fluorescence a sensitive probe for studying molecular environments and dynamics (Fig. 1).

Fluorophores

Fluorophores, also known as fluorescent dyes, are molecules that can re-emit light upon light excitation. They are pivotal in various scientific and medical fields due to their ability to emit fluorescence. When a fluorophore absorbs a photon, its electrons are excited from the ground state to a higher energy state. The electrons then return to the ground state, releasing energy in the form of visible light, a process known as fluorescence. The emitted light is of a longer wavelength (lower energy) compared to the absorbed light, a phenomenon referred to as the Stokes shift. Fluorophores typically consist of conjugated systems with alternating double and single bonds, enabling delocalization of π-electrons. This structure allows them to absorb and emit light efficiently. The properties of fluorophores, such as their excitation and emission wavelengths, quantum yield, and fluorescence lifetime, are highly dependent on their chemical structure. Modifications in the molecular structure can tailor these properties for specific applications [13–15]. Fluorophores are categorized based on their chemical nature and application (Fig. 2).

a) ***Organic Dyes***: These include fluorescein, rhodamine, and cyanine dyes. They are widely used due to their strong fluorescence and diverse spectral properties.
b) ***Inorganic Fluorophores***: Such as quantum dots and rare earth chelates, offer high brightness and photostability, making them suitable for long-term imaging.
c) ***Genetically Encoded Fluorophores***: Green Fluorescent Protein (GFP) and its derivatives are used extensively in biological research for live cell imaging.

Fluorophores are indispensable tools in modern science and technology. Their unique ability to emit light upon excitation allows detailed investigation of environmental pollution detection, biological systems, materials, and chemical environments. Continuous advancements in fluorophore design and application promise to further enhance their utility and impact across various scientific disciplines [16, 17].

Solvent and environmental effects

Fluorophores are highly sensitive to their environment. Factors such as solvent polarity, pH, temperature, and the presence of quenching agents can significantly affect their fluorescence properties. This sensitivity makes them powerful tools for probing the microenvironment in complex systems [18–20].

Solvent Effects Changes in solvent polarity can shift excitation and emission spectra. Solvent effects on the excitation and emission spectra of molecules, particularly fluorescent molecules, are a crucial aspect of photophysics and photochemistry. Changes in solvent polarity can cause significant shifts in these spectra due to interactions between the solvent molecules and the electronic states of the solute (the fluorescent molecule).

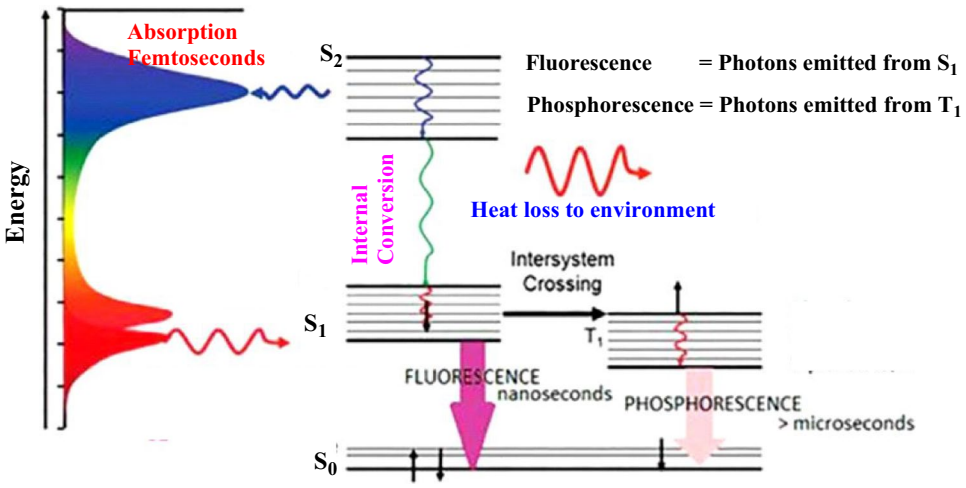

Fig. 1 Jablonski Diagram for Fluorescence and phosphorescence

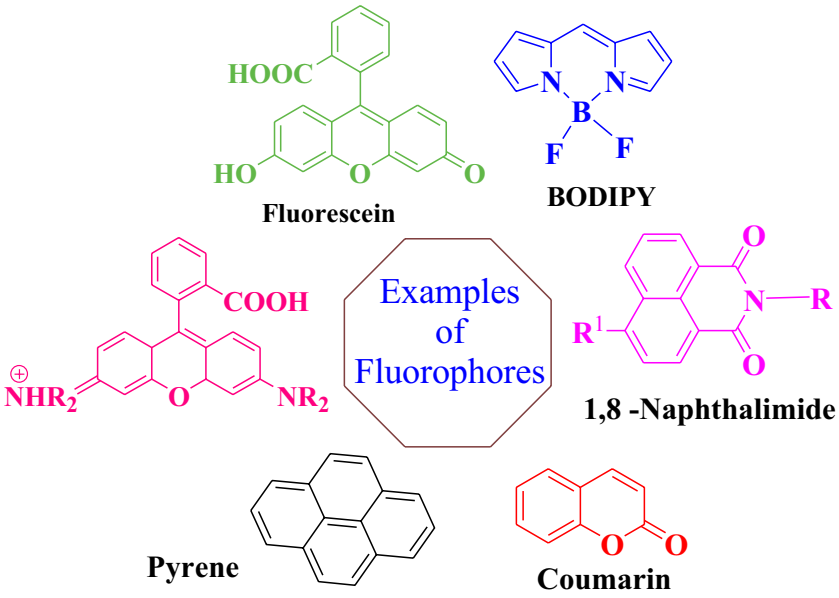

Fig. 2 Types of Fluorophores

pH Sensitivity Certain fluorophores, like fluorescein, have fluorescence properties that vary with pH, useful for measuring pH changes in biological systems.

Temperature Higher temperatures can lead to increased non-radiative decay rates, reducing fluorescence intensity.

Mechanism based fluorescence chemosensors

Photoinduced *Electron* Transfer mechanism (PET)

Photoinduced Electron Transfer (PET) is widely used in the design of fluorescent sensors for detecting protons and metal ions. PET involves the movement of an electron, initiated by light absorption, from an electron-rich donor to an electron-deficient acceptor. When light is absorbed, an electron is promoted from the highest occupied molecular orbital (HOMO) to the lowest unoccupied molecular orbital (LUMO), creating an excited state. The energy required to remove an electron from the highest molecular orbital to the vacuum is called the ionization potential (IP). The excited state has a lower ionization potential than the ground state.

In the excited state, the donor molecule's LUMO is populated, allowing an exothermic electron transfer to the acceptor's LUMO, forming a radical ion pair. Alternatively, if the acceptor molecule is photoexcited, its LUMO is populated, creating a vacancy in the acceptor's HOMO. An exothermic electron transfer from the donor's HOMO to this vacancy then occurs, also generating a radical ion pair. The system can return to its original state by a back electron transfer from the acceptor's LUMO to the donor's HOMO vacancy created during PET (Fig. 3).

A novel receptor, R1, derived from 8-hydroxyquinoline-5-carbaldehyde Schiff-base, has been developed for the selective and sensitive detection of Al^{3+} ions in a 10% (v/v) methanol–water mixture (acetate buffer, pH 4.5), outperforming other metal ions [21]. In its free state, receptor R1 exhibits weak fluorescence at 480 nm when excited at 378 nm. This weak emission is attributed to the photoinduced electron-transfer (PET) effect, where the lone pair electrons from the Schiff-base and quinoline nitrogen atoms quench the fluorescence. Upon the introduction of Al^{3+} ions, there is a significant enhancement in fluorescence, increasing by 30-fold. This dramatic increase in fluorescence is due to the highly efficient chelation-enhanced fluorescence (CHEF) effect when Al^{3+} binds to R1. Other metal cations do not produce a similar enhancement in fluorescence. Fluorescence studies revealed that the stoichiometry of the R1-Al^{3+} complex follows a 1:2 binding mode. The detection limit for Al^{3+} was determined to be below 10^{-7} M (Fig. 4).

A novel quinoline-Schiff base fluorescent receptor, R2, specifically 2-(2-hydroxybenzylidene)hydrazonomethyl) quinolin-8-ol, has been synthesized and thoroughly characterized [22]. Receptor R2 demonstrates exceptional selectivity and sensitivity towards Cu^{2+} ions in a DMSO/H_2O solution (1:1 v/v, 0.01 M Tris–HCl buffer, pH 7.20). Due to intermolecular π–π* charge transfer (CT) transitions, R2 displays two prominent absorption peaks at 299 nm and 352 nm. When Cu^{2+} ions are added, the initially colorless R2 solution turns yellowish-green. In its fluorescence spectrum, R2 exhibits weak fluorescence ($\Phi = 0.049$) at 623 nm upon excitation at 352 nm, attributed to the excited-state intramolecular proton transfer (ESIPT) mechanism. This

weak fluorescence arises from the photoinduced electron-transfer (PET) process from the nitrogen atom near the phenol group to the naphthyl fluorophore, as well as cis–trans isomerization around the C = N bond in R2. Introducing Cu^{2+} ions to R2 significantly enhances fluorescence. The absorption at 352 nm corresponds to the enol form of the probe, while the keto tautomers, resulting from ESIPT from the phenolic hydroxyl to the nitrogen atoms of the Schiff base, are responsible for the stronger emission at 623 nm. The binding constant (K) and stoichiometry of R2 with Cu^{2+} ions were determined to be 3.38×10^{-4} M^{-1} at 299 nm and 3.63×10^{-4} M^{-1} at 352 nm, with a 1:1 binding mode and a detection limit of 8.08 nM (Fig. 5).

A novel fluorescent receptor, R3, identified as 4(1H-benzo[d]imidazol-2-yl)-2-(pyridin-2-yl)quinoline, has been developed for the selective detection of copper ions (Cu^{2+}) in CH_3CN-HEPES buffer solution (pH 7, 10 mM, 9:1 v/v) [23]. The sensing capabilities of R3 were evaluated against various metal ions, including Na^+, Mg^{2+}, K^+, Mn^{2+}, Ca^{2+}, Fe^{2+}, Co^{2+}, Cu^{2+}, Zn^{2+}, Cd^{2+}, Ba^{2+}, Hg^{2+}, and Pb^{2+}. Upon the addition of Cu^{2+} to R3, the fluorescence intensity significantly decreased from $\Phi = 0.239$ to $\Phi = 0.0012$.

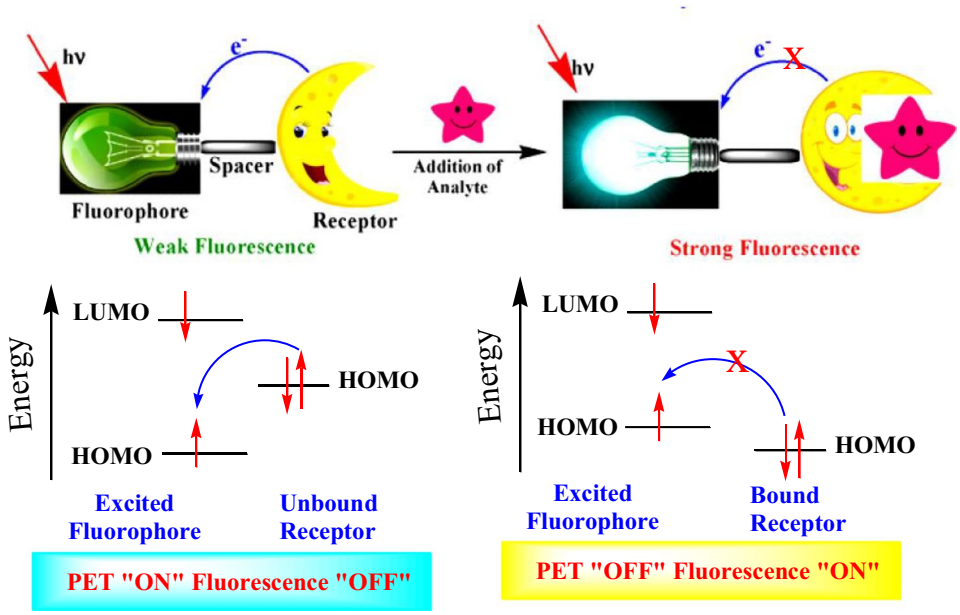

Fig. 3 Photoinduced Electron Transfer mechanism

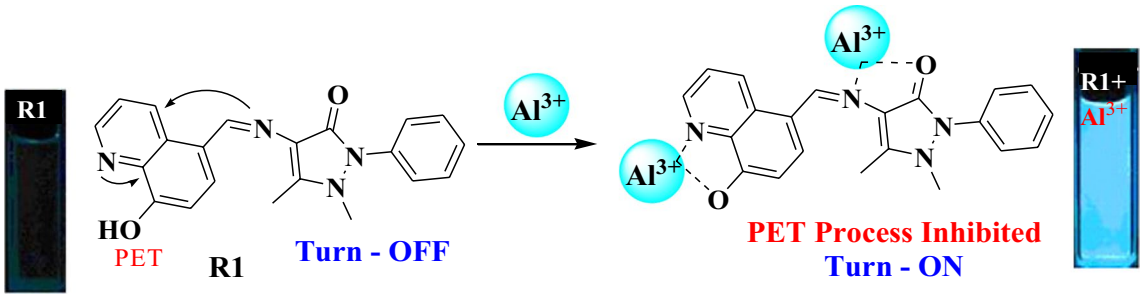

Fig. 4 Sensing mechanism of R1 with Al^{3+} ions

Fig. 5 Structure of R2

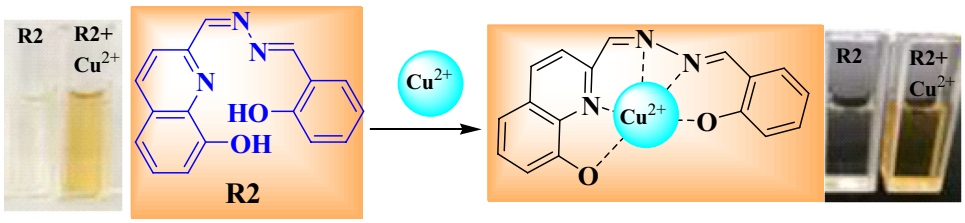

Additionally, the absorption band of R3 at 332 nm diminished and exhibited a slight red shift to 345 nm. As the concentration of Cu^{2+} increased, the absorption band at 345 nm gradually intensified, indicating a typical photoinduced electron transfer (PET) process. In the emission spectrum the free receptor showing an intensity band at 440 nm and the band was declined upon the incremental addition of Cu^{2+} ions. The binding constant, binding stoichiometry and detection limit of R3 with Cu^{2+} were determined to be 3.38×10^{-5} M^{-1}, 1:1, and 1.86 μM, respectively (Fig. 6).

A novel quinoline-based receptor, R4, has been designed and synthesized for the detection of mercury ions (Hg^{2+}). Metal ion recognition studies were conducted using $CHCl_3$/CH_3OH (1:1 v/v) and aqueous organic solvents [24]. Initially, the quinoline moiety exhibited an absorption band at 300 nm, which decreased while a new red-shifted absorption band at 355 nm emerged with increasing Hg^{2+} ion concentration. An isosbestic point was clearly observed at 330 nm. Gradual addition of Hg^{2+} ions to R4 resulted in a significant decrease in emission intensity at 395 nm, accompanied by the appearance of a new emission peak centered at 482 nm. This shift is attributed to the formation of an excimer between the quinoline moieties, which are brought closer together due to strong Hg^{2+} chelation within the R4 cavity. The association constant and stoichiometry for the Hg^{2+} complex were determined to be 2.15×10^{-4} M^{-1} and 1:1, respectively. Additionally, the presence of Zn^{2+} and Cd^{2+} ions enhanced the fluorescence spectrum, which is due to the inhibition of the photoinduced electron transfer (PET) process between the excited state of quinoline and the binding site (Fig. 7).

A novel fluorescent receptor, R5, based on a quinoline moiety, has been developed and examined for its sensing capabilities towards Zn^{2+} and Cd^{2+} in an aqueous solution (25 mM HEPES, 0.1 M $NaNO_3$, pH 7.4) [25]. In water, free receptor R5 exhibits weak fluorescence ($\Phi = 0.023$). Upon the addition of Zn^{2+}, a significant fluorescence enhancement is observed at 373 nm and 509 nm. The enhancement at 509 nm is attributed to the binding of Zn^{2+} to the imidic acid

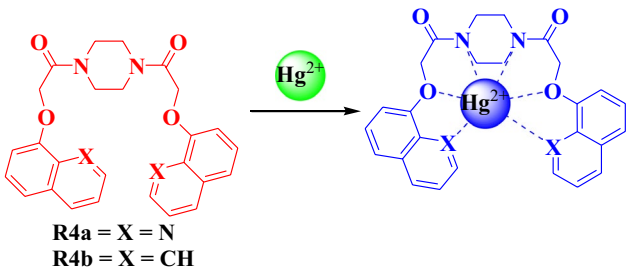

Fig. 7 Structure of R4

tautomer of R5, which results in an expanded conjugated system. This binding blocks the intra-molecular photoinduced electron transfer (PET) process, leading to increased fluorescence. When Cd^{2+} is added to R5, turn-on fluorescence is observed at 373 nm. The amide tautomer of R5 binds with Cd^{2+}, also blocking the intra-molecular PET process and causing an increase in fluorescence intensity at 373 nm. The dissociation constants for the Zn^{2+} and Cd^{2+} complexes were found to be 3.36 nM and 30.62 nM, respectively. The stoichiometry for the binding of receptor R5 with both Zn^{2+} and Cd^{2+} was determined to be 1:1 (Fig. 8).

A novel quinoline-coupled pyrazole receptor, R6, has been developed as a colorimetric and fluorescent sensor for the selective detection of Zn^{2+} in an EtOH-H_2O solution (1:1 v/v, 50 mM HEPES, pH 7.2) [26]. Upon the addition of Zn^{2+} to R6, the absorption bands at 280 nm and 323 nm gradually decrease, and a new absorption band appears at 380 nm, accompanied by a noticeable color change from colorless to pale yellow. Other metal ions such as Na^+, K^+, Cu^{2+}, Cd^{2+}, Ni^{2+}, Hg^{2+}, Pb^{2+}, Co^{2+}, Ca^{2+}, Mn^{2+}, Cr^{3+}, Ba^{2+}, Mg^{2+}, Fe^{2+}, Fe^{3+}, Al^{3+}, Zr^{2+}, Ce^{3+}, and Ag^+ do not induce any visual, absorption, or emission changes in R6. The free receptor R6 exhibits weak fluorescence ($\Phi = 0.019$) with emission at 408 nm. Upon interaction with Zn^{2+}, the fluorescence shifts slightly from 408 to 418 nm and is significantly enhanced ($\Phi = 0.214$). These spectral changes are due to the inhibition of the photoinduced electron transfer (PET) process and the

Fig. 6 Structure of R3

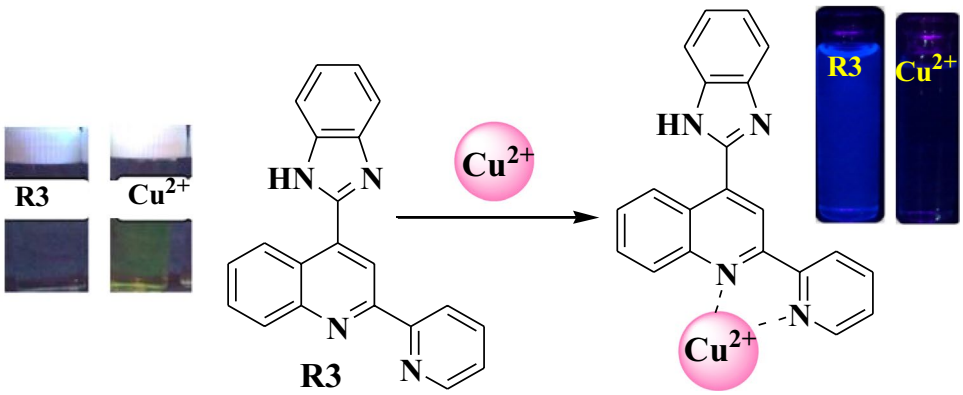

restricted C = N isomerization mechanism. The binding constant, stoichiometry, and detection limit of R6 with Zn^{2+} are calculated to be 1.88×10^{-4} M^{-1}, 1:1, and 2.9 nM, respectively. The receptor R6 has also been successfully utilized for selective imaging of Zn^{2+} in living cells (Fig. 9). Cadmium (Cd^{2+}) typically forms complexes with larger coordination numbers (up to 8) and prefers softer ligands like sulfur. In contrast, Zn^{2+} usually forms complexes with lower coordination numbers (4 to 6) and favors harder ligands like oxygen and nitrogen. The distinct preferences in ligand types and coordination environments allow for the differentiation between Cd^{2+} and Zn^{2+} binding.

A quinoline-Schiff base fluorescent receptor, R7, has been reported for the selective and sensitive detection of Zn^{2+} in ethanol, even in the presence of various interfering metal ions [27]. When receptor R7 is excited at 375 nm, it exhibits weak fluorescence due to the photoinduced electron transfer (PET) phenomenon from the lone pair electrons of the Schiff-base nitrogen atom to the benzene moiety of R7. However, upon the addition of Zn^{2+}, a significant fluorescence enhancement at 450 nm is observed. This enhancement occurs because the complexation of R7 with Zn^{2+} inhibits the PET phenomenon. Among the various interfering metal ions tested, only Cr^{3+} and Hg^{2+} caused fluorescence quenching due to the photoinduced electron and energy transfer processes. The detection limit, stoichiometry, and binding constant of receptor R7 with Zn^{2+} were determined to be 3.5 μM, 1:1, and 2.3×10^{-4} M^{-1}, respectively (Fig. 10).

A quinoline-based turn-on chemosensor, receptor R8, demonstrates high selectivity and sensitivity for Zn^{2+} in a MeOH-Tris buffer (7/3 v/v, pH 7.3) compared to other interfering metal ions [28]. Due to the photoinduced electron transfer (PET) process involving the non-bonding electron pairs of nitrogen atoms in the picolinohydrazide moiety, receptor R8 exhibits weak fluorescence. However, upon the addition of various metal ions, a significant fluorescence enhancement is observed around 490 nm specifically when Zn^{2+} binds to R8. This binding also results in a noticeable color change from colorless to light green. The fluorescence enhancement due to Zn^{2+} is attributed to the inhibition of the PET effect from the electron-donating picolinohydrazide

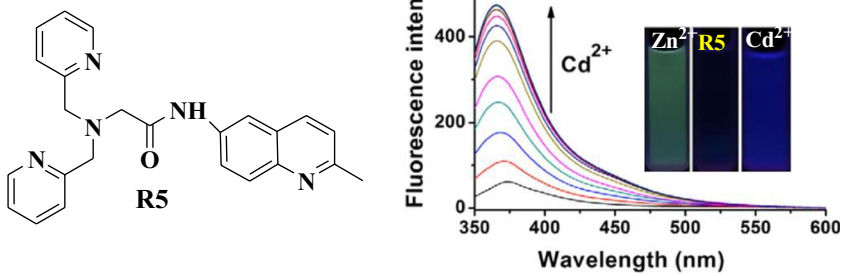

Fig. 8 Structure of R5 and its fluorescence behaviour towards Cd^{2+}

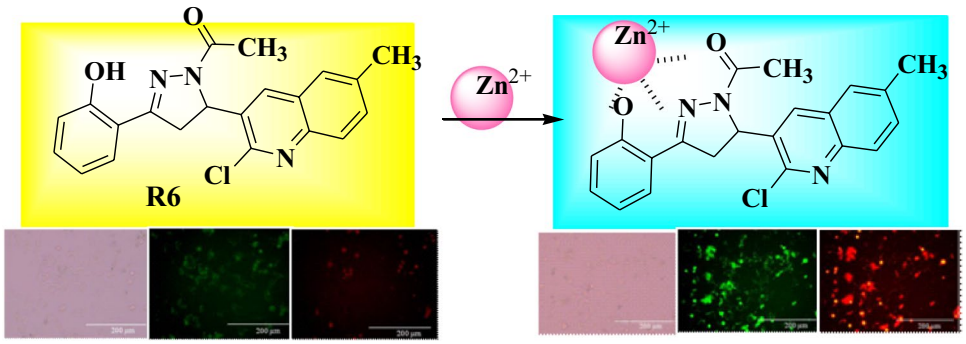

Fig. 9 Structure of R6 and its fluorescence bioimaging

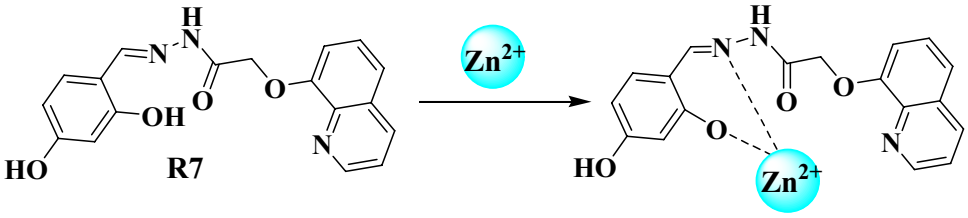

Fig. 10 Structure of R7 and its sensing mechanism towards Co^{2+} and Zn^{2+}

moiety to the electron-accepting 8-aminoquinoline moiety. Additionally, the R8-Zn^{2+} complex can serve as a new cascade chemosensor for sequential detection of pyrophosphate (PPi) and sulfide (S^{2-}), leading to a fluorescence "OFF–ON–OFF" switching pattern. The binding constant and stoichiometry of receptor R8 with Zn^{2+} are determined to be 6.7×10^{5} M^{-1} and 1:1, respectively. The detection limits of R8 are calculated to be 3.8×10^{-8} M for Zn^{2+}, 3.7×10^{-7} M for PPi, and 4.9×10^{-7} M for S^{2-} (Fig. 11).

A novel 7-hydroxyquinoline-based fluorescent receptor, R9, has been developed for the selective detection of Zn^{2+} in HEPES buffer (25 mM HEPES, 0.1 M $NaClO_4$, 5% (v/v) DMSO, pH 7.4) [29]. Receptor R9 features a methoxy group at the 7-position of the quinoline ring. When excited at 320 nm, R9 exhibits weak fluorescence emission at 393 nm. However, upon the addition of Zn^{2+}, the fluorescence emission intensity increases significantly ($\Phi=0.556$). This enhanced fluorescence is due to the inhibition of the photoinduced electron transfer (PET) mechanism. The binding mode of R9 with Zn^{2+} was determined to be 1:1, and the dissociation constant was found to be 0.117 nM. R9 also demonstrates higher selectivity for Zn^{2+} over Cd^{2+}. Additionally, a cell-permeable derivative of R9 can be utilized for imaging Zn^{2+} in living cells using two-photon microscopy (Fig. 12).

Two fluorescein-quinoline based derivatives, R10a (2-[2-chloro-6-hydroxy-3-oxo-5-(quinolin-8-ylaminomethyl)-3H-xanthen-9-yl]benzoic acid) and R10b (2-[6-hydroxy-3-oxo-4,5-bis-(quinolin-8-ylaminomethyl)-3H-xanthen-9-yl]benzoic acid), were designed, synthesized, and characterized [30]. Both dyes exhibit excellent selectivity for Zn^{2+} in a buffer solution containing 50 mM PIPES and 100 mM KCl at pH 7. Free receptors R10a and R10b show weak fluorescence (R10a: $\Phi=0.024$; R10b: $\Phi=0.50$). Upon binding with Zn^{2+}, a 33-fold fluorescence enhancement at 524 nm is observed, with quantum yields of 0.78 for R10a and 0.71 for R10b. In the absorption spectrum, a blue shift from 505 to 498 nm occurs upon Zn^{2+} binding with R10a and R10b. These changes indicate a perturbation of the fluorescein π system, likely due to Zn^{2+} coordination to the phenol group. Single-photon and multiphoton microscopy confirm that both R10a and R10b are cell-permeable and responsive to Zn^{2+} in vivo (Fig. 13).

A fluorescent receptor, R11, conjugated with quinoline and benzimidazole, has been synthesized for the highly selective detection of Zn^{2+} in a HEPES-buffered CH_3CN/H_2O solution (1:1 v/v, pH 7.0), effectively discriminating against interference from other metal ions [31]. Receptor R11 exhibits two absorption bands at 213 nm and 372 nm. Upon addition of Zn^{2+}, there is an enhancement in absorption at both 213 nm and 372 nm, accompanied by a noticeable color change from pale yellow to intense yellow. Initially, the emission spectrum of receptor R11 shows weak fluorescence emission at 425 nm, which is attributed to the intramolecular photoinduced electron transfer (PET) process and the unrestricted torsional rotation between the C–C single bond that covalently links the quinoline and benzimidazole units. However, upon addition of Zn^{2+}, a prominent enhancement in emission is observed, resulting in intense yellowish-green

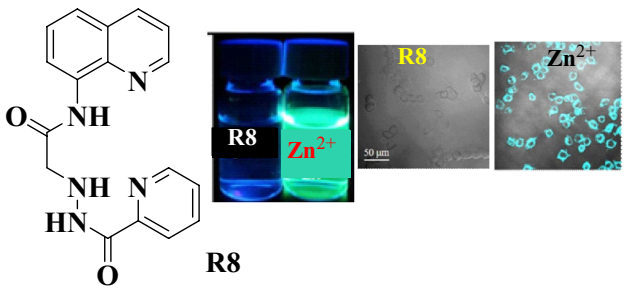

Fig. 11 Structure of R8

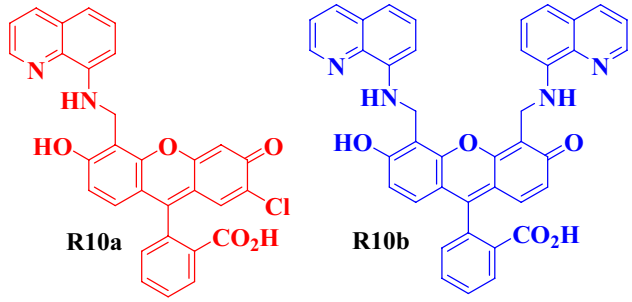

Fig. 13 Structure of R10a-b

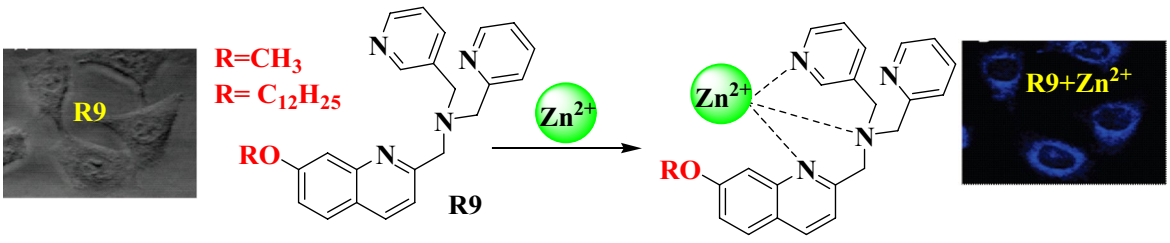

Fig. 12 Structure of R9 and Zn.$^{2+}$ in living cells (imaging)

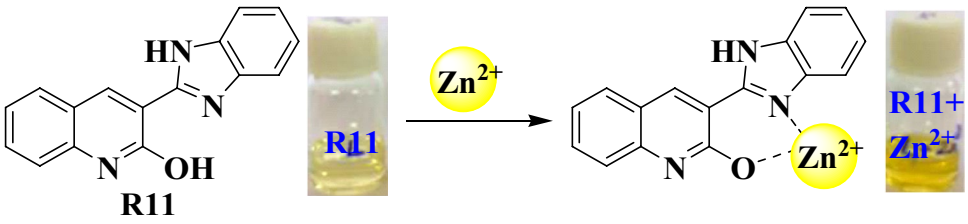

Fig. 14 Structure of R11 and its sensing mechanism towards Zn^{2+}

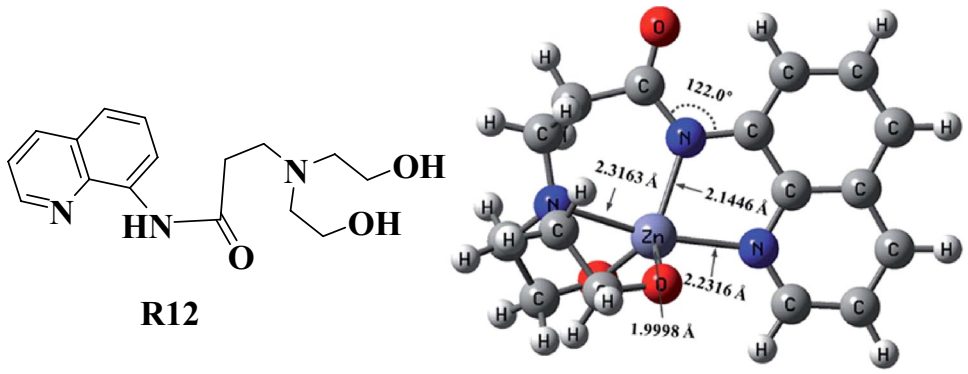

Fig. 15 Structure of R12 and its complex structure with Zn^{2+}

fluorescence with emission maxima at 425 nm. This fluorescence enhancement is attributed to the inhibition of the PET process between the quinoline-benzimidazole conjugate and the restriction of rotation around the C–C single bond linking the quinoline and benzimidazole rings. The association constant, stoichiometry, and detection limit are calculated to be 1.53×10^4 M^{-1}, 1:1, and 0.15 µM, respectively (Fig. 14).

A water-soluble fluorescent chemosensor, receptor R12, based on a quinoline derivative, was synthesized for the selective detection of zinc ions in a 100% aqueous buffer solution [32]. Upon excitation at 350 nm, receptor R12 exhibits weak fluorescence with a low quantum yield ($\Phi = 0.00084$). This weak fluorescence is attributed to the photo-induced electron transfer (PET) process involving the nonbonding electron pair of tertiary nitrogen, which can transfer an electron to the excited fluorophore, thus quenching the fluorescence. However, upon addition of Zn^{2+}, a significant fluorescence enhancement at 500 nm is observed, possibly due to the inhibition of the PET process. The binding constant, detection limit, and binding mode are determined to be $K = 1.4 \times 10^4$ M^{-1}, 4.48 µM, and 1:1, respectively (Fig. 15).

A simple receptor, R13, based on quinoline, specifically 3-((2-(dimethylamino)ethyl)amino)-N-(quinolin-8-yl) propanamide, has been synthesized for detecting Zn^{2+} in a mixture of MeCN and bis–tris buffer solution (3:7 v/v) [33]. The UV–vis absorption spectrum of R13 exhibits two absorption bands at 240 nm and 310 nm. Upon the addition of Zn^{2+} to R13, these absorption bands red-shift to 257 nm and 367 nm, respectively. Additionally, three distinct isosbestic points are observed at 246 nm, 283 nm, and 336 nm, indicating the clear conversion of free receptor R13 to a zinc

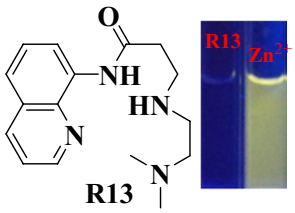

Fig. 16 Structure of R13

complex. Exciting free receptor R13 at 370 nm results in weak fluorescence emission at 523 nm. However, upon the addition of Zn^{2+}, a significant fluorescence enhancement is observed around 525 nm. The detection limit and stoichiometry of R13 for Zn^{2+} are calculated to be 76 µM and 1:1, respectively (Fig. 16).

Intramolecular charge transfer (ICT)

Intramolecular Charge Transfer (ICT) offers an alternative approach to designing toxic ions detection based chemosensors. The ICT fluorescent molecular probe consists of a fluorophore, a strong electron donor, and a strong electron acceptor, which together form a robust push–pull electron system. Upon photoexcitation, charge transfer occurs from the electron donor to the electron acceptor. When the identification group of the ICT fluorescence probe interacts with the target, it alters the push–pull electron effect within the fluorophore. This interaction either weakens or strengthens the intramolecular charge transfer, resulting in changes to the fluorescence spectrum, such as blue shifts or red shifts (Fig. 17).

Receptor R14, a quinoline-based fluorescence sensor appended with bisphenol A, serves as a multi-analyte

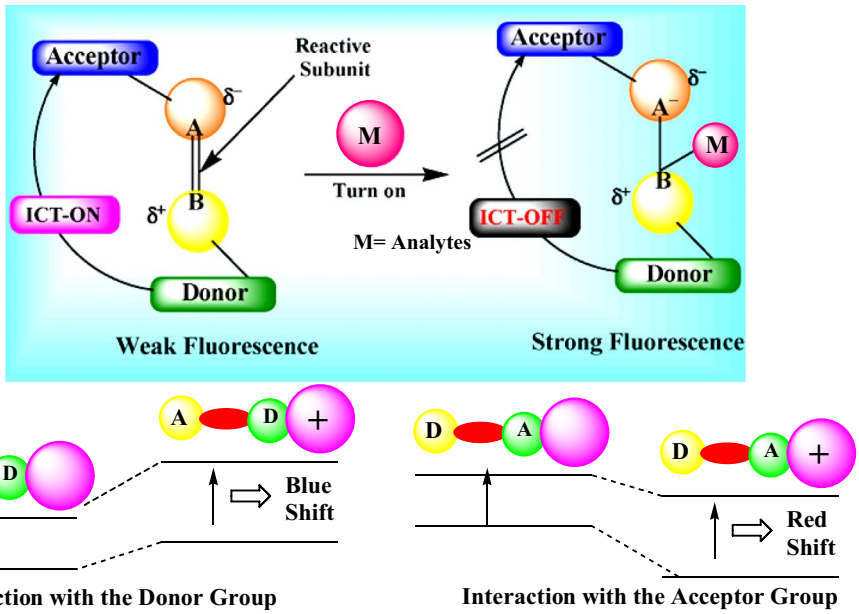

Fig. 17 Intramolecular Charge Transfer mechanism

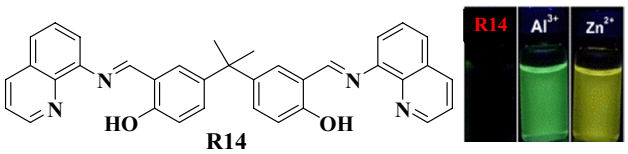

Fig. 18 Structure of R14 & and color changes under UV light

detector in an ethanol–water mixture (v/v = 9/1) [34]. Upon the addition of various metal ions to R14, only Zn^{2+} and Al^{3+} induce yellow and green fluorescence emissions, respectively. Initially, R14 exhibits weak fluorescence emission at 550 nm, attributed to the turn-off behavior of the receptor caused by isomerization of the C = N double bond and the intramolecular charge transfer (ICT) effect. However, interaction with Zn^{2+} and Al^{3+} may inhibit the C = N isomerization and ICT effect in R14, leading to a chelation-enhanced fluorescence effect. Consequently, upon addition of Zn^{2+} and Al^{3+} to R14, strong fluorescence enhancements are observed at 560 nm (Φ = 0.172) and 530 nm (Φ = 0.239), respectively. The binding constants, detection limits, and stoichiometries are determined to be $2.32 \pm 0.21 \times 10^{10}$ M^{-2} (Zn^{2+}), $0.73 \pm 0.17 \times 10^{10}$ M^{-2} (Al^{3+}), 3.56 μM (Zn^{2+}), 1.14 μM (Al^{3+}), and 1:1 binding mode (Fig. 18).

A novel fluorescence receptor, N-(quinolin-8-yl)-2-(quinolin-8-yloxy)acetamide R15, incorporating both 8-aminoquinoline and 8-hydroxyquinoline units, was designed and synthesized for the dual detection of Zn^{2+} and Cd^{2+} [35]. The receptor's sensing capabilities in ethanol were evaluated. Excitation of R15 at 329 nm resulted in a weak emission peak at 410 nm with a quantum yield (ϕ) of 0.008. Introduction of Cd^{2+} ions led to a significant increase in fluorescence intensity (ϕ = 0.16) at the same excitation wavelength, indicating a 1:1 binding ratio. This fluorescence enhancement is attributed to the photoinduced electron transfer (PET) mechanism. In the presence of various interfering ions, Zn^{2+} caused a notable red shift in the emission spectrum to 486 nm (ϕ = 0.019), also exhibiting a 1:1 binding ratio. This red shift and fluorescence enhancement are due to the internal charge transfer (ICT) mechanism. The binding constants for R15 with Zn^{2+} and Cd^{2+} were determined to be 1.8×10^4 and 9.8×10^5, respectively (Fig. 19).

A coumarin-quinoline based receptor, R16, has been crafted for Zn^{2+} detection in a solvent mixture of $CH_3CN:H_2O$ (1:3, v/v) buffered with 10 mM HEPES at pH 7.2 [36]. This yellow receptor R16 undergoes a visual color change to pale red and transitions from green to yellow under UV light. Absorption studies reveal that R16 alone exhibits a

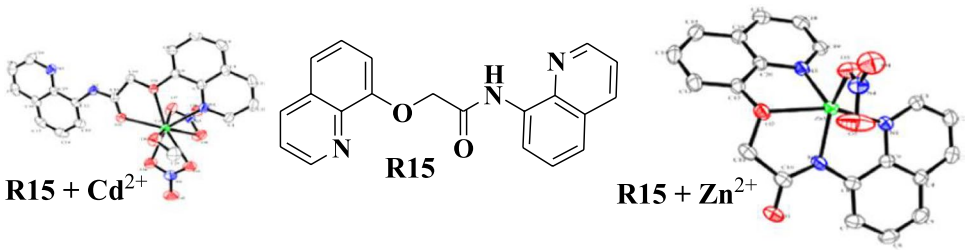

Fig. 19 Structure of R15 and its complex structure with Cd^{2+} and Zn^{2+}

peak at 442 nm, indicative of intramolecular charge transfer (ICT) from the 7-diethylaminocoumarin to the 8-hydroxyquinoline unit. Adding Zn^{2+} ions to R16 results in a gradual decrease in the 442 nm absorbance, while a new peak emerges at 531 nm. Correspondingly, fluorescence at 516 nm diminishes, accompanied by a red-shift to a new emission band at 556 nm. This substantial 40 nm red-shift is attributed to the enhanced electron-withdrawing capability of the triazole-R16 complex upon Zn^{2+} coordination, which facilitates the ICT process from 7-diethylaminocoumarin to the triazole-modified R16. The detection limit for Zn^{2+} was determined to be 48.1 nM (Fig. 20).

A fluorescence receptor, R17, derived from 2-(2-nitrostyryl)-8-methoxyquinoline, has been synthesized for the detection of Zn^{2+} in a $CH_3CN–H_2O$ (9:1, v/v) medium [37]. The absorption spectrum of R17 shows a prominent band at 279 nm, attributable to the π–π* transition of the styrylquinoline moiety, and a weaker, broader band at 340 nm in CH_3CN. When excited at 319 nm, R17 exhibits a weak fluorescence emission at 480 nm, which is likely due to internal charge transfer (ICT) from the methoxy donor group to the nitrostyryl acceptor group. Upon the addition of Zn^{2+}, there is a marked enhancement in fluorescence, explained by the inhibition of ICT from the methoxy group to the nitrostyryl group. The binding constant of R17 with Zn^{2+} is 8.35×10^{11} M, with a 1:1 stoichiometry and a detection limit of 3.8 μM (Fig. 21).

The quinoline-based receptor 2-(hydroxymethyl)-4-methyl-6-((quinolinyl-8-imino)methyl)phenol (R18) exhibits exceptional selectivity and sensitivity for Zn^{2+} in a Tris–HCl buffer (50 mM, pH 7.54) within a THF-H_2O (9:1, v/v) medium [38]. When various metal ions are introduced to R18, Zn^{2+} uniquely induces a decrease in the absorption band at 338 nm and the appearance of a new band at 455 nm, accompanied by a noticeable color change from colorless to yellow. This new absorption peak is attributed to the coordination of Zn^{2+} with R18. The emission spectrum of R18, excited at 455 nm, shows a weak fluorescence at 515 nm with a quantum yield of $\Phi = 0.006$. Upon addition of Zn^{2+}, there is a 14-fold increase in fluorescence intensity, a red shift in the emission maximum to 565 nm, and an enhanced quantum yield of $\Phi = 0.045$. R18 binds to Zn^{2+} through a 1:2 stoichiometry, forming a five-membered chelate ring with the aminoquinoline moiety via two nitrogen atoms and a six-membered chelate ring involving the Schiff base –C = N and Ar-OH groups. This chelation enlarges the conjugated system, thereby reducing the energy gap between the n and π* orbitals (Fig. 22).

Salicylaldimine and aminoquinoline-based derivatives R19a-d have been successfully synthesized and are reported for their selective detection of Zn^{2+} in an ethanol–water (9:1, v/v) medium [39]. When various metal ions, including Zn^{2+}, Mn^{2+}, Ba^{2+}, Hg^{2+}, Ni^{2+}, Cu^{2+}, Co^{2+}, Pb^{2+}, Mg^{2+}, Cd^{2+}, Fe^{2+}, Cr^{3+}, Al^{3+}, Fe^{3+}, Li^{+}, K^{+}, and Na^{+}, are introduced to R19a-d, receptor R19a exhibits a significantly enhanced emission peak at 535 nm upon interaction with Zn^{2+} and at 439 nm with Al^{3+}. Receptors R19b and R19c demonstrate remarkable selectivity towards Zn^{2+}, showing no response

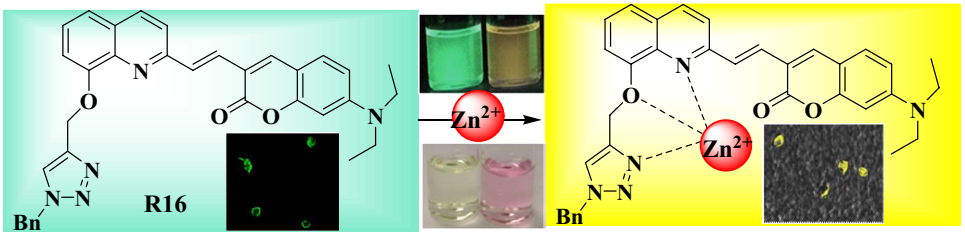

Fig. 20 Structure of R16 and its sensing mechanism towards Zn^{2+}

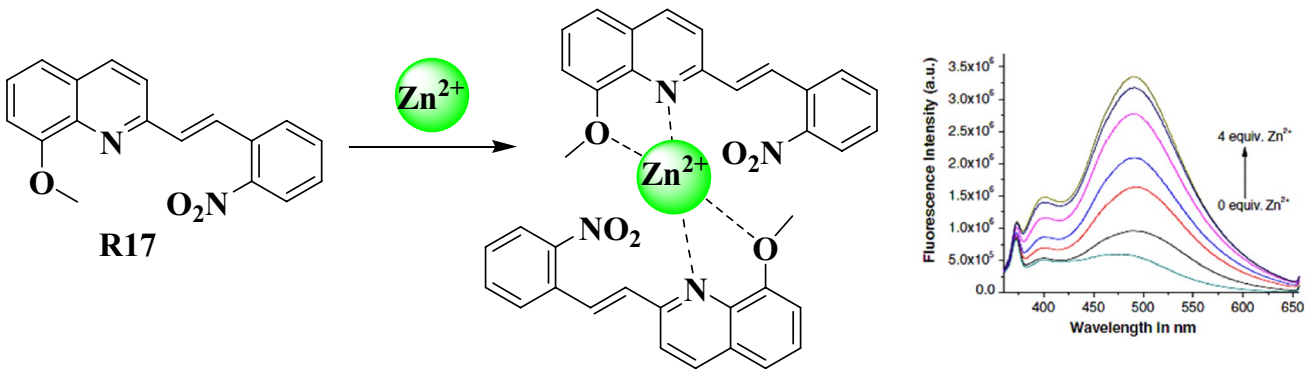

Fig. 21 Structure of R17

Fig. 22 Structure of R18 and its colorimetric changes

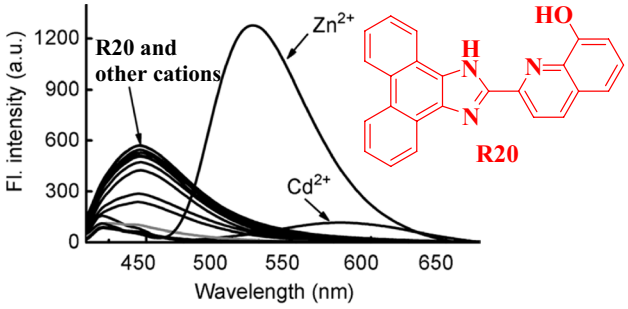

Fig. 24 Structure of R20 and the fluorescence studies of R20 with all the metal ions

to Al^{3+}. The selective fluorescence enhancement by Zn^{2+} is attributed to chelation-enhanced fluorescence (CHEF) effects, where the deprotonation of the amido –NH and phenolic –OH groups initiates an internal charge transfer (ICT) process. The detection limits for Zn^{2+} with receptors R19a-b are found to range from 0.024 to 0.431 µM, with a 1:1 stoichiometry. The association constants for these sensors are estimated to range between 7.0×10^3 and 1.2×10^4 M^{-1} (Fig. 23).

A straightforward fluorescence receptor, R20, for detecting Zn^{2+} and Cd^{2+} was designed and synthesized by condensing phenanthrene-9,10-dione with 8-hydroxyquinoline-2-carbaldehyde in a mixture of ethanol and dichloromethane [40]. The sensing properties of receptor R20 were explored in the presence of various metal ions, including Al^{3+}, Ca^{2+}, Mg^{2+}, Na^{+}, Fe^{2+}, Fe^{3+}, Mn^{2+}, Ni^{2+}, Co^{2+}, Cr^{3+}, Cu^{2+}, Hg^{2+}, Pb^{2+}, Zn^{2+}, and Cd^{2+}, in a water/DMF (7:3, v/v) solution. The free receptor R20 exhibits a primary emission band around 445 nm when excited at 340 nm. The presence of ions such as Fe^{2+}, Fe^{3+}, Ni^{2+}, Mn^{2+}, Co^{2+}, Cu^{2+}, Pb^{2+}, and Cr^{3+} causes significant fluorescence quenching. Conversely, the addition of Zn^{2+} induces a pronounced shift in fluorescence from 445 to 520 nm. A more substantial redshift, from 445 to 580 nm, occurs upon the introduction of Cd^{2+}. These considerable redshifts suggest that Zn^{2+} and Cd^{2+} interact with the electron donor sites in receptor R20, facilitating an effective internal charge transfer (ICT) (Fig. 24).

A simple Schiff-base quinoline-based receptor, R21 ((E)-2-Methoxy-N-((quinolin-2-yl)methylene)aniline), has been reported for its selective, sensitive, and reversible detection of Zn^{2+} and Hg^{2+} in a DMSO–H_2O solution (1/99 v/v) [41]. The absorption maxima of R21 were observed at 293 nm, 292 nm, and 295 nm in DMA, DMF, and DMSO, respectively, corresponding to π–π* transitions and intramolecular charge transfer (ICT) processes. The fluorescence intensity of receptor R21 gradually decreased and red-shifted to 473 nm with increasing DMSO fraction in the mixed solvent system. The strong emission of R21 in polar solvents can be attributed to π*–π transitions of non-aggregated molecules. In contrast, the decreased fluorescence intensity and red shift were due to the aggregation-caused quenching effect, shifting the fluorescence band from 413 to 473 nm. Upon the addition of Zn^{2+} to the R21 solution, a remarkable enhancement in fluorescence intensity was observed, along with the generation of new peaks at 565 nm. Similarly, the addition of Hg^{2+} triggered emission at 530 nm (yellowish-green), slightly less intense than that observed with Zn^{2+}. The detection limits for Zn^{2+} and Hg^{2+} with R21 were calculated to be 0.011 µM and 0.040 µM, respectively (Fig. 25).

Carboxamidoquinoline-based fluorescence probes R22a-b were synthesized and reported as selective sensors for Zn^{2+} in a methanol–water solution (1:9 v/v) with an ionic strength of 0.1 (KCl). These probes demonstrated selectivity for Zn^{2+} over other interfering metal ions such as Ag^{+}, Ca^{2+}, Mg^{2+}, Pb^{2+}, Na^{+}, K^{+}, and Fe^{3+} [42]. The presence of Cu^{2+}, Co^{2+}, and Ni^{2+} resulted in fluorescence quenching of

Fig. 23 Structure of R19a-d

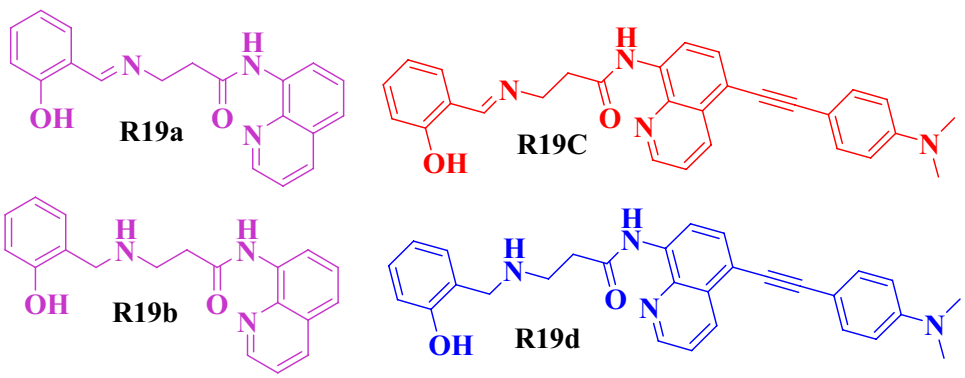

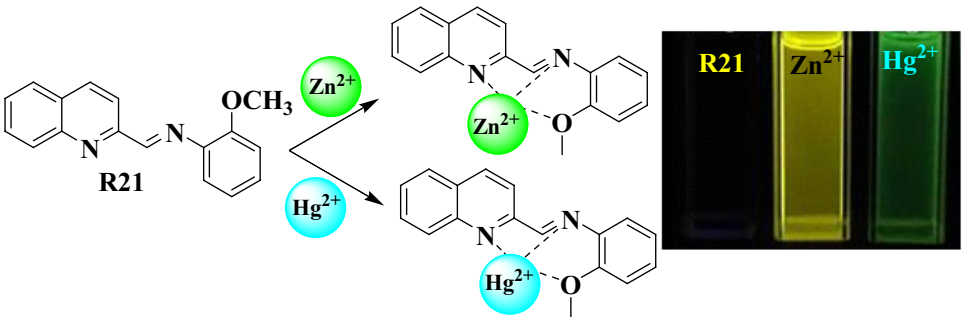

Fig. 25 Structure of R21

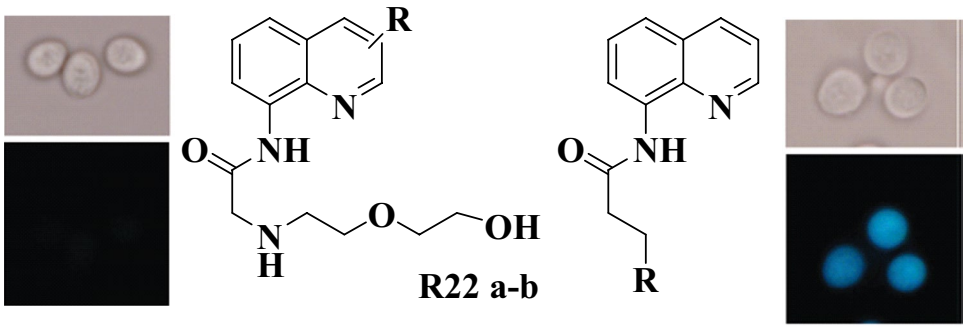

Fig. 26 Structure of R22a-b and its cell imaging studies

the receptors, attributed to energy transfer from the photo-excited quinoline ring to the empty d-orbitals of these metal ions. Upon the addition of Zn^{2+}, R22a-b exhibited a significant fluorescence enhancement due to the deprotonation of the carboxamido group. In living cells, the blue-green emission gradually increased, indicating that the receptor is membrane-permeable and capable of signaling the presence of intracellular Zn^{2+} (Fig. 26).

A carboxamidoquinoline-based fluorescence receptor, R23, featuring an alkoxyethylamino chain, was designed to evaluate its sensing capabilities for various metal ions in a Tris–HCl (0.01 M) solution (methanol/water, 1:9 v/v, pH 7.22) [43]. Upon the addition of increasing amounts of Zn^{2+} to R23, an approximately eightfold increase in fluorescence quantum yield and a 75 nm red-shift from 440 to 515 nm ($\Phi = 7.96$) in fluorescence emission were observed, along with a noticeable blue-green emission visible to the naked eye. The association constant and stoichiometry for the R23-Zn^{2+} complex were determined to be 6.7×10^6 M^{-1} and 1:1, respectively. In acidic conditions, R23 exhibited no fluorescence emission due to the protonation of its amino group. However, as the pH increased from 6.1 to 11.8, R27 showed the highest sensing ability under physiological pH conditions (Fig. 27).

A novel quinoline-based fluorescent receptor, R24, has been reported for the selective sensing of Zn^{2+} in an aqueous solution (ethanol/water = 1:1, v/v) [44]. Receptor R24 exhibited an absorption band at 235 nm and a broad band around 311 nm. Upon the addition of Zn^{2+}, the absorbance at

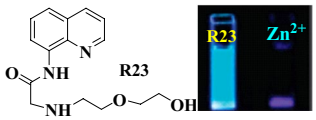

Fig. 27 Structure of R23

240 nm and 311 nm decreased, while new absorption peaks appeared at 262 nm and 363 nm, with isosbestic points at 250 nm and 331 nm. In the fluorescence spectrum, the free receptor showed an emission band at 407 nm ($\lambda_{ex} = 330$ nm; $\Phi = 0.018$). Introducing Zn^{2+} to receptor R24 resulted in a remarkable red-shifted enhanced fluorescence from 407 to 499 nm (92 nm) with a quantum yield of 0.082. This enhanced fluorescence is attributed to the deprotonation process of carboxamidoquinoline and the internal charge transfer (ICT) mechanism. The intramolecular electron-transfer process is activated upon metal ion binding, leading to increased fluorescence emission (Fig. 28).

A ratiometric fluorescent sensor, R25, based on carboxamidoquinoline with a carboxylic acid group, has been synthesized and reported for the selective detection of Zn^{2+} in a tris–HCl buffer (ethanol/water = 1:1, v/v, pH 7.24) medium [45]. Among sixteen metal ions tested, receptor R25 exhibits its exceptional selectivity towards Zn^{2+}, displaying selective fluorescence responses. With the incremental addition of Zn^{2+} into R25, the emission band at 402 nm decreases while that at 484 nm increases (13-fold; 82 nm red-shift), with an iso emission point appearing near 411 nm. The

Fig. 28 Structure of R24

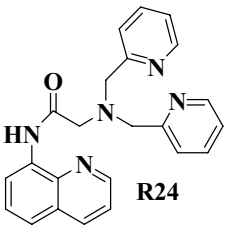

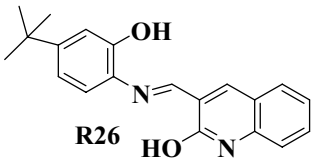

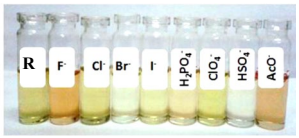

Fig. 30 Structure of R26

absorption spectrum of receptor R25 reveals an absorption peak at 239 nm and a broad band around 306 nm. Absorption experiments demonstrate a 43 nm red-shift from 306 to 349 nm upon zinc binding. The stoichiometry and detection limit of R25-Zn^{2+} were calculated to be 1:1 and 27 μM, respectively. Additionally, R25 has been successfully utilized for determining Zn^{2+} levels in both tap and river water samples (Fig. 29).

A novel quinoline-based fluorescence receptor, R26, was developed as a dual sensor for acetate (AcO^-) and fluoride (F^-) among various anions in a DMSO solvent medium [46]. Upon the addition of F^- and AcO^- to R26 in DMSO, a significant color change from light yellow to orange-brown was observed. This color change is attributed to the intramolecular charge transfer (ICT) process occurring between the phenolic oxygen and the electron-withdrawing quinoline ring, facilitated by the formation of a hydrogen-bonded complex between the hydroxyl groups of R26 and F^- and AcO^-. The free receptor exhibited two absorption bands at 303 nm (-CH = N; π-π*) and 400 nm, indicative of the intramolecular charge transfer (ICT) mechanism (ketoamine–phenolimine). Upon the addition of F^- and AcO^-, a new charge transfer band at approximately 530 nm appeared, indicating the formation of a host–guest complex between the receptor and the anions. The binding constants and stoichiometry of R26 with F^- and AcO^- were calculated to be 2.39×10^5 M^{-1} (F^-), 2.18×10^5 M^{-1} (AcO^-), and 1:1, respectively (Fig. 30).

Excited state intramolecular proton transfer mechanism

In the ESIPT mechanism, molecules exhibit dual emission characteristics. The excited enol form (E*) leads to short-wavelength (normal) emission, while the excited keto form (K*) results in longer wavelength emission (ESIPT emission). The spectral properties of ESIPT fluorophores are influenced by factors such as the donor and acceptor units within the molecule, hydrogen bonding behavior, the acidity or basicity of the solvent, and the rotamerization process. Additionally, the fluorescence properties of ESIPT fluorophores can be adjusted by altering the surrounding medium (Fig. 31).

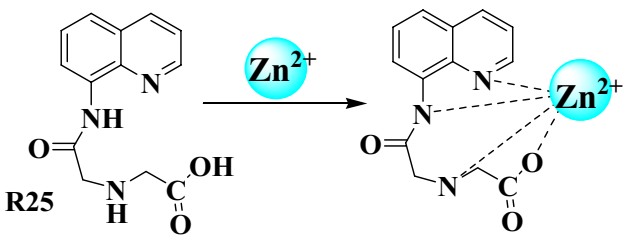

Fig. 29 Structure of R25

A novel fluorescence receptor, R27, based on ESIPT (Excited-State Intramolecular Proton Transfer), has been developed for the detection of HOCl [47]. When the free receptor R27 is excited at 360 nm, it exhibits a prominent emission band at 515 nm, attributed to the ESIPT process, resulting in a large Stokes shift of 155 nm. Upon the addition of NaOCl, the fluorescence intensity at 515 nm significantly decreases, accompanied by the appearance of a new emission peak at 585 nm. The detection limit for HOCl was calculated to be 40 nM. Receptor R27 holds potential for monitoring both exogenous and endogenous HOCl and can be localized in the endoplasmic reticulum of living cells (Fig. 32).

A straightforward flavone-based receptor, R28, was synthesized to leverage the Excited-State Intramolecular Proton Transfer (ESIPT) process for ratiometric detection of hydrogen polysulfides [48]. The receptor exhibits high selectivity and sensitivity towards hydrogen polysulfides, boasting a low detection limit of 0.63 μM. Featuring a 2-fluoro-5-nitrobenzoic acid group, R28 effectively inhibits the intramolecular ESIPT process, resulting in the blue fluorescence of the neighboring naphthalene unit. In the presence of H_2S, the enol form of the probe converts to the conjugated keto form, leading to a substantial 90 nm red-shift in fluorescence emission from 450 to 540 nm. The receptor has been successfully employed for exogenous H_2S detection and imaging via dual emission channels in living Hela cells (Fig. 33).

A novel naphthalimide-based receptor, R29, was devised, synthesized, and disclosed for the ratiometric detection of Al^{3+} through the inhibition of ESIPT in a H_2O/CH_3CN (1:9; v/v) solvent system [49]. In the absorption spectrum, R29 exhibits two distinct charge transfer bands at 340 nm and 460 nm. Upon excitation at 460 nm, R29 displays two emission bands at 510 nm and 610 nm. The introduction of Al^{3+} into R29 induces a color change from orange to yellow,

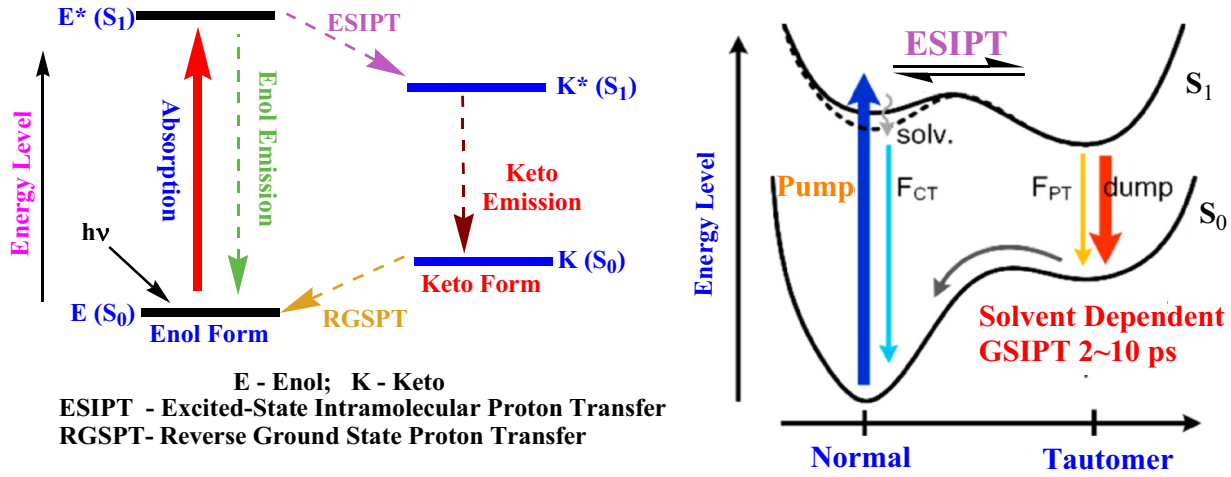

Fig. 31 Excited state intramolecular proton transfer mechanism

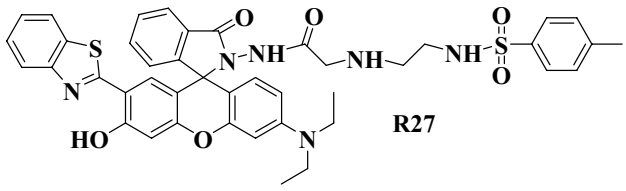

Fig. 32 Structure of R27

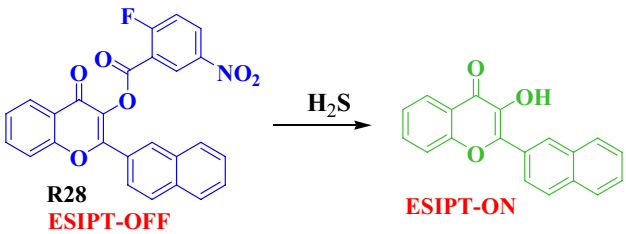

Fig. 33 Structure of R28

with the charge transfer band at 460 nm increasing ratiometrically. Under UV light, R29-Al^{3+} emits blue-green light, transitioning from yellow, and displays an enhanced emission band at 540 nm. Furthermore, the receptor enables the ratiometric detection of F^-, manifesting a color change from orange to purple, with an emission band observed at 570 nm. The detection limits for receptor R29 with Al^{3+} and F^- were determined to be 32 nM and 75 µM, respectively (Fig. 34).

C. Shang and fellow researchers introduced a fluorescence receptor, R30, based on hydroxyanthraquinones, and investigated the ESIPT mechanism by altering electronic groups [50]. The maximum absorption peaks of these receptors experienced a red shift. Notably, the addition of electron-withdrawing substituents induced a substantial Stokes shift. Analyses of FMOs and NBO population confirmed the charge recombination around the proton donor and acceptor, strengthening hydrogen bonding and providing further momentum for ESIPT behavior (Fig. 35).

A carbazole-conjugated Schiff base serves as a sensitive fluorescent receptor (R31) for detecting Al^{3+} ions in an ethanol–water (1:1, v/v) medium [51]. The receptor exhibits a new absorption band at 531 nm, arising from the transfer of lone pairs of electrons from nitrogen/oxygen of the receptor to the metal ion. Initially, the receptor emits weak fluorescence due to the isomerization of the C=N bond in the excited state via excited-state intramolecular proton transfer (ESIPT). However, upon the introduction of Al^{3+} ions, enhanced fluorescence emission is observed, indicating the disruption of the ESIPT feature. The association constant, binding mode, and detection limit of receptor R31 with Al^{3+} were calculated to be 5×10^4 M^{-1}, 1:1, and 2.59 µM, respectively (Fig. 36).

A novel Schiff base fluorescence receptor, R32, namely (E)-4-methyl-2-((2-(9-(naphthalen-1-yl)-8-(thiophen-2-yl)-9H-purin-6-yl)hydrazono)methyl)phenol, was designed and presented for the detection of Al^{3+} in DMSO/H_2O (9/1, v/v, pH = 7.4) [52]. Initially non-fluorescent, the receptor exhibits an enhanced emission intensity at 462 and 488 nm upon interaction with Al^{3+}. This increase in fluorescence of receptor R32 may be ascribed to the inhibition of the PET and ESIPT processes induced by Al^{3+}. The detection limit and binding mode were determined to be 82 nM and 1:1, respectively. R32 efficiently detects trace amounts of Al^{3+} in test strips and living HeLa cells (Fig. 37).

A Schiff base fluorescence receptor, R33, incorporating coumarin was synthesized to facilitate an ESIPT transfer process for detecting Hg^{2+} and Pb^{2+} ions in a HEPES buffer solution [53]. Upon the addition of Hg^{2+}, the yellow color of the receptor shifted to colorless and exhibited very weak cyan fluorescence emission at 470 nm. This diminished

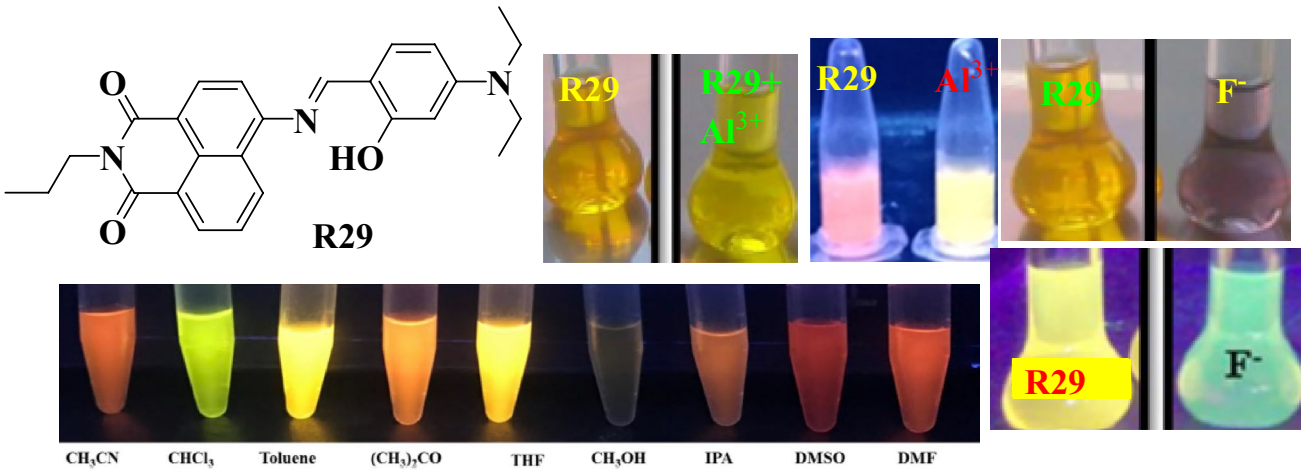

Fig. 34 Structure of R29 and its visual and fluorescence color change

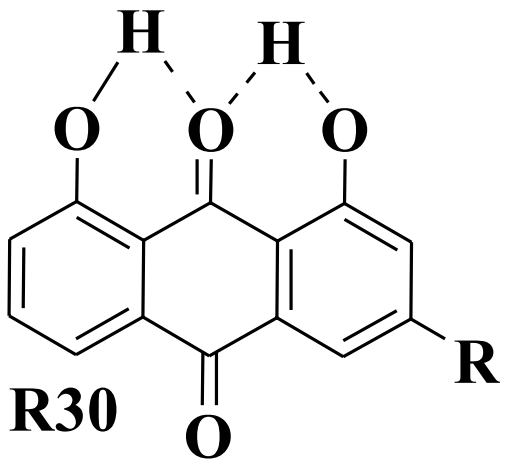

Fig. 35 Structure of R30

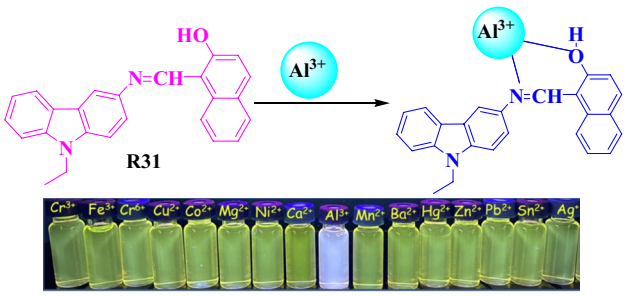

Fig. 36 Structure of R31 and its sensing mechanism towards Al^{3+}

fluorescence emission can be attributed to the phenolic-oxygen atoms and imine nitrogen distributing the lone pair of electrons, thereby inhibiting ESIPT and activating PET

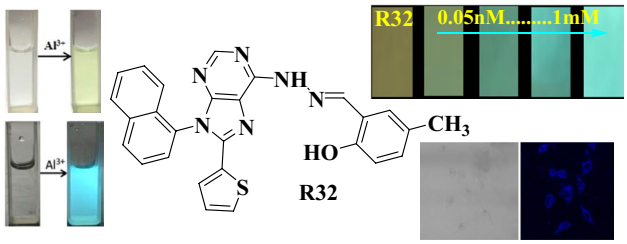

Fig. 37 Structure of R32 and its fluorescence images

processes. The detection limits were determined to be 8.3 and 10.5 nM for Hg^{2+} and Pb^{2+} ions, respectively (Fig. 38).

A novel Schiff base receptor, R34, featuring benzimidazole conjugation, 1-[[(1H-1,3-benzodiazol-2-yl)imino]methyl]naphthalen-2-ol, demonstrated remarkable selectivity towards Cu^{2+} and exhibited a robust fluorescence enhancement at 504 nm in a CH_3CH_2OH-PBS (v/v = 1:1, pH = 7.0) mixed solution [54]. Initially, R34 displayed very weak fluorescence emission at 365 nm. However, with an increase in water content in R34, the fluorescence emission intensity gradually rose from 497 to 504 nm. The binding stoichiometry and detection limit were calculated to be 2:1 and 0.814 nM, respectively (Fig. 39).

A dinitrophenyl-based Schiff base fluorescence receptor R35 act as an efficient detection of Zn^{2+} in a DMSO-H_2O solvent mixture. Due to the ESIPT mechanism the receptor shows a weak fluorescence emission at 530 nm when excites the receptor at 340 nm [55]. Upon the addition of Zn^{2+} into R35 an enhanced fluorescence was noticed at 530 nm. The enhanced fluorescence emission is due to the inhibition of the excited state intramolecular proton transfer mechanism. The red-colored receptor solution turned yellow color in the presence of zinc ions. The binding constant, stoichiometry,

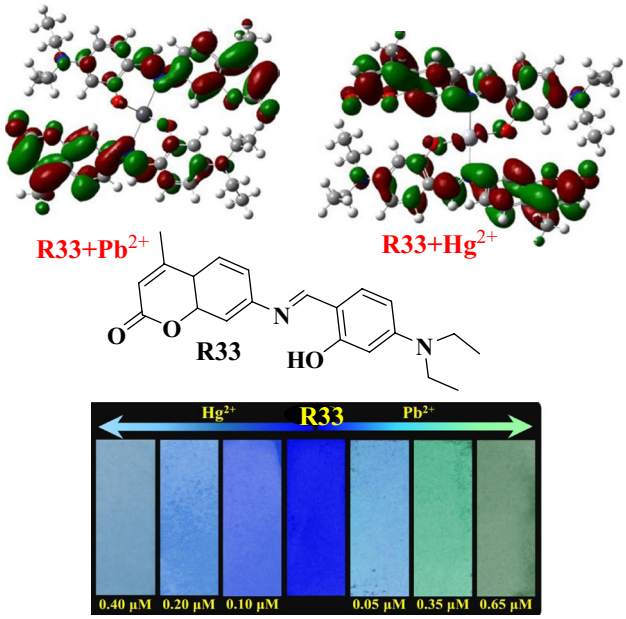

Fig. 38 Structure of R33 and sensing test strips

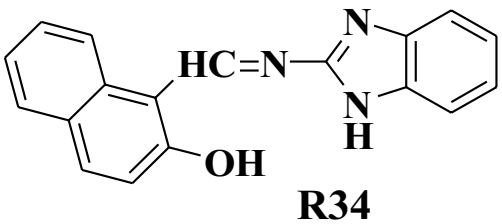

Fig. 39 Structure of R34

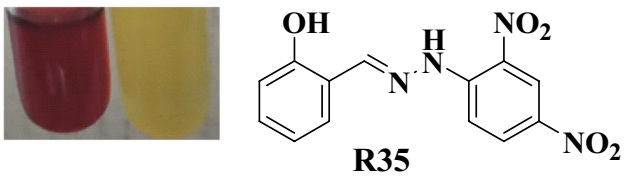

Fig. 40 Structure of R35

and detection limit were found to be 6.35×10^7 M^{-1}, 1:1, and 0.11 nM, respectively (Fig. 40).

Dual detection-based hydrazone Schiff base fluorescence receptor R36 has been synthesized and characterized [56]. By adding Cu^{2+} into R36 its shows 410 nm and the decrease of fluorescence emission intensity at 532 nm with an appearance of emission band at 570 nm. In the presence of F^- ions the receptor shows a new absorption band at 513 nm and an emission band at 532 nm. The –NH unit in the Schiff base receptor is the proper H-bond donor which can act as a selective sensor for F^- ions. The detection limits of R36 towards

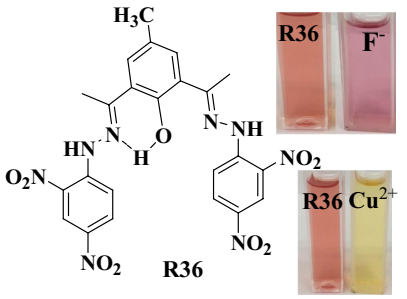

Fig. 41 Structure of R36

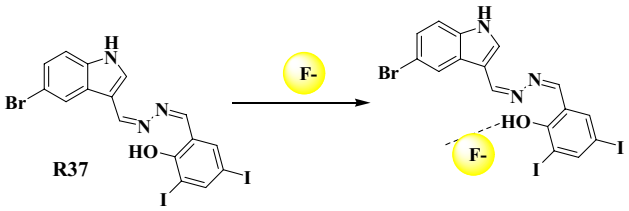

Fig. 42 Structure of R37 and its sensing mechanism towards F^-

Cu^{2+} and F^- were calculated to be 3.51 µM and 3.26 µM, respectively with a 2:1 demultiplexer (Fig. 41).

A novel Schiff base receptor, R37, has been developed for the detection of F^- and tryptamine ions in a DMSO-H_2O (9:1, v/v) medium, utilizing both colorimetric and fluorimetric methods [57]. In the presence of tryptamine, R37 exhibits enhanced fluorescence at 433 nm, while a band at 533 nm decreases in intensity due to the inhibition of ESIPT. Conversely, in the presence of fluoride ions, the intensity of the band at 430 nm increases, while the band at 555 nm decreases, owing to the ESIPT mechanism. Fluorescence analysis was conducted in live cell studies using HeLa cells and Zebrafish embryos (Fig. 42).

A fluorescence Schiff base receptor, R38, has been developed and synthesized for the selective detection of N_2H_4 and CN^- ions [58]. Hydrazine leads to the quenching of the bright green fluorescence of R38, while cyanide induces a change in the bright green fluorescence to an orange-red color. The receptor operates through the ESIPT process and a resonance-assisted hydrogen bonding-coupled structure. Upon coordination with N_2H_4 and CN^-, the ESIPT process of R38 is disrupted. In test strip studies, R38 demonstrates significant color changes upon interaction with N_2H_4 and CN^- ions (Fig. 43).

An efficient fluorescence receptor R39 has been developed by using Bis(2-aminophenyl) ether and salicylaldehyde [59]. The receptor is well characterized with FTIR, ^1H NMR, ^{13}C NMR, and mass spectroscopic analysis. Upon the addition of Al^{3+} ions into R39, fluorescence turn-on at the large Stokes shifted wavelength 528 fold. The turn-on

Fig. 43 Structure of R38

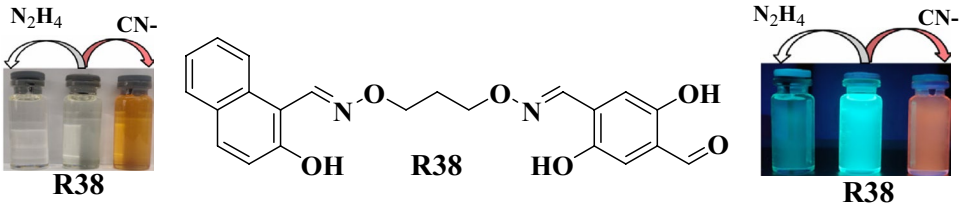

Fig. 44 Structure of R39

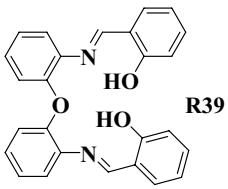

fluorescence is due to the electron-releasing-substituent on the phenol rings and exhibits an ESIPT mechanism. The detection limit and stoichiometry were calculated to be 5.48 nM and 1:1 binding mode (Fig. 44).

Fluorescence resonance energy transfer (FRET)

A fluorescent probe based on the FRET mechanism can link two fluorophores (donor and acceptor) within a single molecule. The donor (D) absorbs radiation at the excitation wavelength and transfers this energy to the acceptor (A), which then emits it at a longer wavelength. If the emission spectrum of the donor overlaps with the absorption spectrum of the acceptor, non-radiative energy transfer from D to A can occur. When D is excited, the fluorescence emission of A can be observed as a result of this energy transfer (Fig. 45).

A quinoline-conjugated benzothiazole derivative linked with rhodamine-6G receptor R40 act as an efficient FRET-based single molecular switch for detecting Fe^{3+} ions in a CH_3OH/H_2O solution (2/3, v/v, pH = 7.2) [60]. It exhibits an immediate fluorescence ratiometric response specific to Fe^{3+}, enabling easy naked-eye detection of Fe^{3+}. The R40 shows high selectivity for Fe^{3+} compared to other environmentally significant cations, including Fe^{2+}. The ratiometric response is primarily driven by the FRET mechanism. Coordination of Fe^{3+} with the nitrogen atom of the benzothiazole moiety, the nitrogen and oxygen atoms of hydroxyquinoline, and the nitrogen atom of the rhodamine–ethylene diamine moiety, along with electron transfer from the benzothiazole, leads to the opening of the spiro ring. The detection limit and binding mode of the receptor with Fe^{3+} were determined to be 0.53 nM and 1:1, respectively (Fig. 46).

Y. Wang and his team reported that hydrazone-bearing 1,8-naphthalimide and pyrrole moieties (R41) act as the first ratiometric fluorescent sensor for Cu^{2+}, utilizing hydrolysis via Cu^{2+}-promoted electrophilic substitution [61]. In the presence of Cu^{2+} ions in a CH_3CN/H_2O solution (9:1, v/v, pH = 7.40), receptor R41 shows a decrease in absorbance at 480 nm and a red shift from 335 to 350 nm, changing its color from orange to colorless. R41 alone exhibits a significant red fluorescence emission band at 620 nm. Upon the addition of Cu^{2+}, fluorescence intensity increases, and a new emission band appears at 545 nm, distinguishing Cu^{2+} from other cations such as Ag^+, Al^{3+}, Ca^{2+}, Cd^{2+}, Co^{2+}, Cr^{3+}, Fe^{3+}, Hg^{2+}, K^+, Mg^{2+}, Mn^{2+}, Na^+, Ni^{2+}, Pb^{2+}, and Zn^{2+}. The detection limit of R41 for Cu^{2+}

Fig. 45 Fluorescence resonance energy transfer

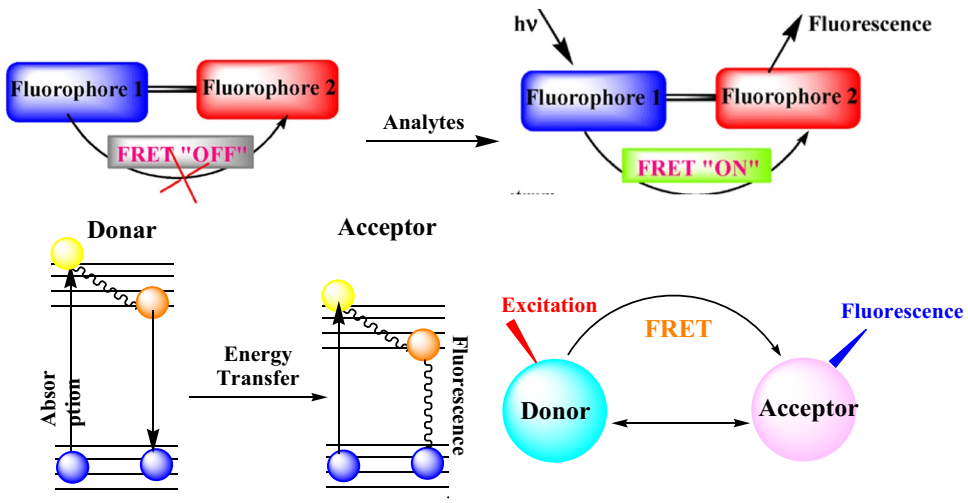

ions is 1.50 μM, with a binding mode of 1:1. Additionally, receptor R41 can be used to image intracellular Cu^{2+} in living cells (Fig. 47).

Shen and colleagues created a ratiometric and colorimetric fluorescent receptor, R42, that specifically detects SO_3^{2-}/HSO_3^- ions in an EtOH/PBS buffer solution (10 mM, pH 7.4, v/v = 3/7) [62]. When excited at 405 nm, it exhibits a fluorescence shift from red to green, with a response time of less than 3 min. R42 features a large Stokes shift and a broad emission window, effectively preventing interference between the two fluorescence emission channels. Furthermore, its excellent luminescence properties enabled its initial use as a fluorescent donor for a FRET receptor, enhancing the diversity of donors available. The detection limit for R42 was determined to be 39 nM. The receptor is capable of detecting both exogenous and endogenous sulfites in living cells, making it suitable for use in cellular and mouse imaging (Fig. 48).

A novel ratiometric fluorescent receptor, R43, has been synthesized for detecting Hg^{2+} ions in environmental and various biological samples. The receptor employs a covalent connection of two fluorophores via lipoic acid to enable fluorescence resonance energy transfer (FRET) [63]. In the molecular structure of receptor, acridone serves as the energy donor, 1,8-naphthalimide functions as the energy acceptor, and a dithioacetal group acts as the reaction site for Hg^{2+}. The intact receptor predominantly displays green fluorescence from the 1,8-naphthalimide acceptor moiety. Upon exposure to Hg^{2+} ions, the dithioacetal linkage between acridone and 1,8-naphthalimide is cleaved, disrupting FRET and resulting in a bright blue fluorescence emission from acridone. This process allows for the ratiometric fluorescent detection of Hg^{2+}. The detection limit is calculated to be 30 nM. Additionally, this receptor has been successfully applied to detect Hg^{2+} in actual samples

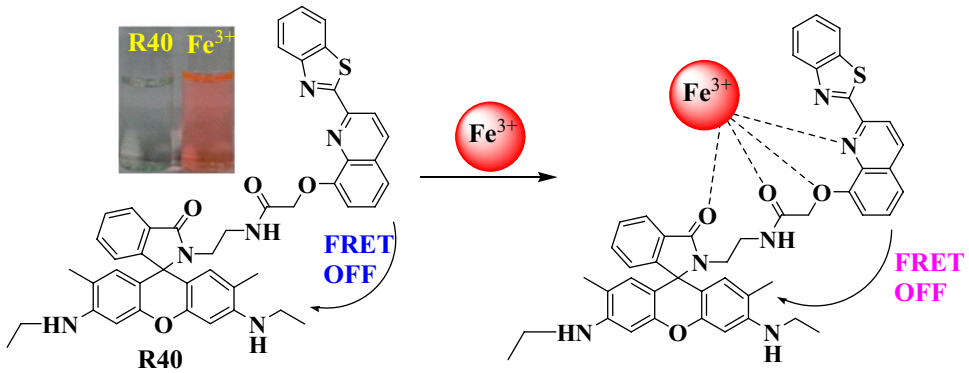

Fig. 46 Structure of R40 and its sensing mechanism with Fe^{3+} ions

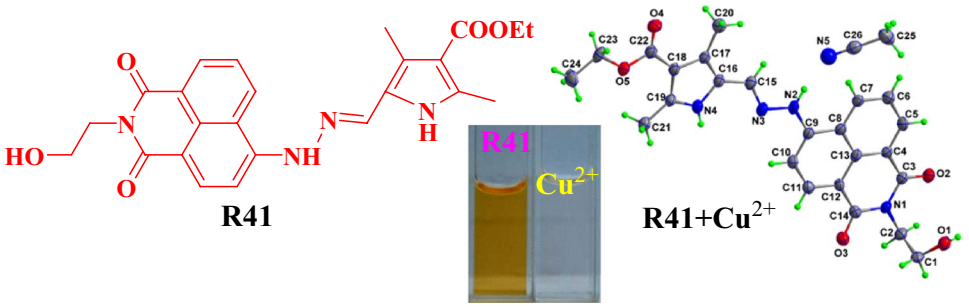

Fig. 47 Structure of R41 and R41-Cu^{2+} ions

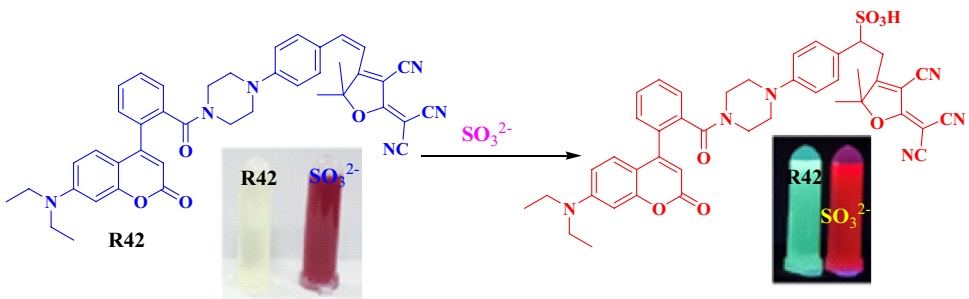

Fig. 48 Structure of R42 and its sensing mechanism with SO_3^{2-} ions

and to image a variety of organisms, demonstrating its broad application potential (Fig. 49).

Liu et al., reported a novel ratiometric fluorescent receptor R44 based on 1,8-naphthalimide-rhodamine for the selective & sensitive detection of Fe^{3+}/Hg^{2+} ions in ethanol/PBS buffer (1:1, v/v, pH = 7.4) solution [64]. Receptor R44 with Hg^{2+} ions exhibits typical FRET signal from pyridine-naphthalimide moiety to rhodamine moiety with the lowest detection limit of 2.72×10^{-6} M. However, in the presence of Fe^{3+} ions the receptor R44 shows ratiometric detection behavior via PET process combined with the classical ring-opening sensor system with the detection limit of 5.7×10^{-7} M. Receptor R44 emitted bright yellow fluorescence in solid state & the maximum wavelength was 538 nm. The dye-doped Si-nanoparticles emit strong green fluorescence, the maximum fluorescence emission wavelength was 495 nm & further rainforced the AIE effect (Fig. 50).

N-Z Xu & coworkers designed & synthesized a novel receptor R45 based on 1,8-naphthalimide group & rhodamine B for the selective & sensitive detection of Hg^{2+} ions [65]. Upon addition of Hg^{2+} ions to receptor R45 reveals a significant color change from colorless to pink & a light to orange fluorescence change. The receptor R45 was selectively sensed with Hg^{2+} based on the fluorescence resonance energy transfer (FRET) mechanism. receptor R45 shows a typical FRET signal from the 1,8-naphthalimide group to the rhodamine group, a new emission peak appears at 585 nm & the emission peak at 381 nm decreases in the fluorescence spectrum with 1:1 binding stiochiometry. The detection limit was found to be 0.059 μM & the calculated association constant was 2.75×10^5 M^{-1} (Fig. 51).

A Rhodamine B-Quinoline conjugate receptor R46 selectively detects Bi^{3+} by colorimetric and fluorescence methods based on CHEF assisted FRET process in DMSO:

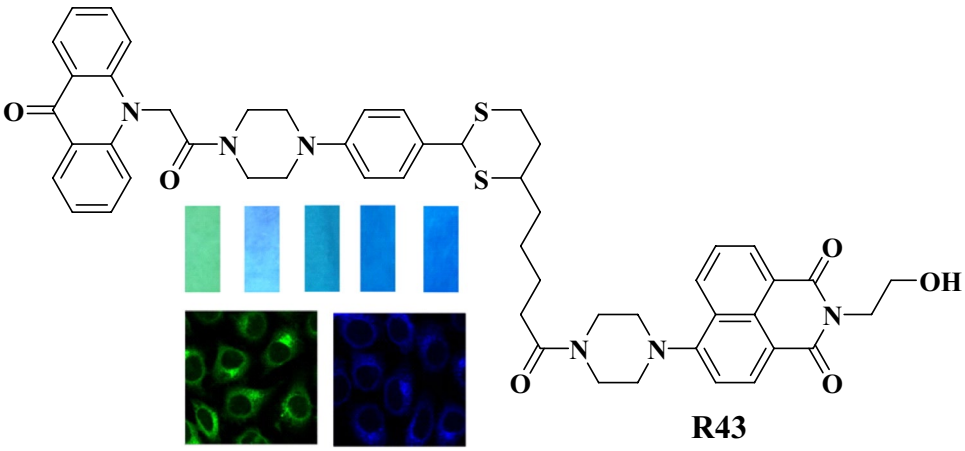

Fig. 49 Structure of R43

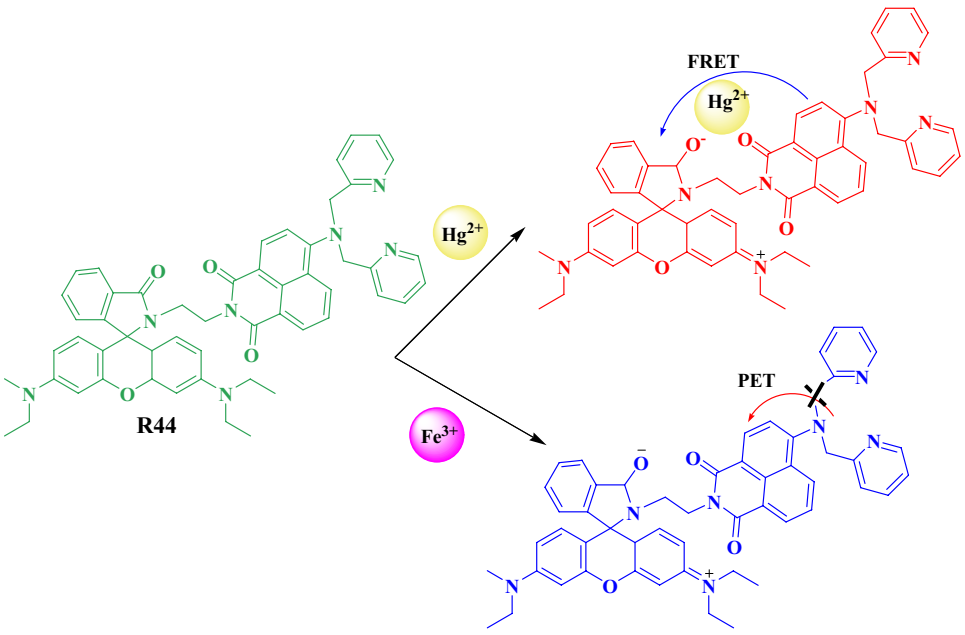

Fig. 50 Structure of R44 and its sensing mechanism with Hg^{2+} & Fe^{3+} ions

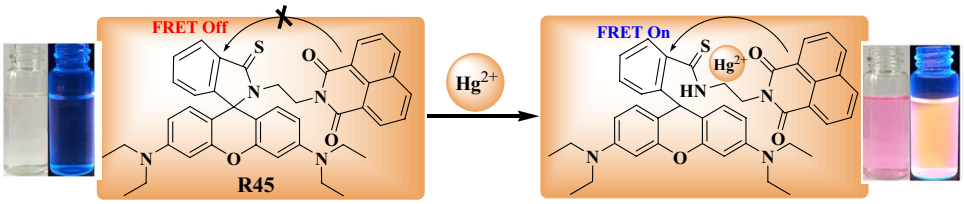

Fig. 51 Structure of R45 and its sensing mechanism with Hg^{2+} ions

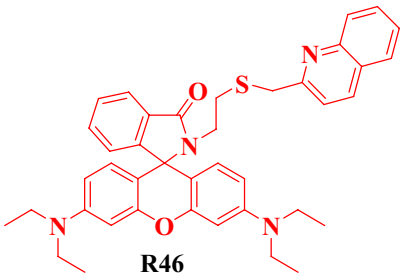

Fig. 52 Structure of R46

water (1:1, v/v) [66]. Upon the gradual addition of Bi^{3+} the absorbance at 322 nm increases (1 μM) and increasing the concentration (> 1 to 1000 μM) of Bi^{3+} gradually decreases this absorbance while a new band that appears at 566 nm. A weak fluorescence emission was noticed for free receptor at 597 nm upon the excitation of 525 nm. In the presence of Bi^{3+} the emission intensity along with ~ 30 fold increase was noticed at 597 nm (Φ = 0.59). The binding constant, stoichiometry and detection limit of R46 with Bi^{3+} was calculated to be 2.1×10^5, 1:1 and 0.05 μM, respectively. Receptor R46 can efficiently images intra cellular Bi^{3+} in SiHa cell line. (Fig. 52).

Rhodamine-based fluorescent receptor R47 has been developed for the selective and sensitive detection of Pd^{2+} metal ions in aqueous media MeCN-H_2O (50:50 v/v, 25 °C) [67]. A rhodamine-BODIPY Förster resonance energy transfer (FRET)-pair receptor R47 has been incorporated with a piperazine linker and an O-N-S–N pod and ligand for specific recognition of Pd^{2+} ion. A bright strong green emission was observed for all cations except Au^{3+} and Pd^{2+} in the UV light under 360 nm. The emission of Au^{3+} was quenched after binding to R47; it did not trigger the opening of lactam to give the characteristic red emission of rhodamine; only Pd^{2+} was able to "turn-on" R47 to give intense red emission. Upon reacting with Pd^{2+}, the green colour emission at 515 nm decreased while the red colour emission at 600 nm was increased. Imaging of Pd^{2+} and GSH in live A549 cells was demonstrated, indicating the utility of receptor as a reliable analytical tool for the detection in aqueous media and cell imaging of Pd^{2+} and biothiols (Fig. 53).

A FRET based ratiometric fluorescent receptor R48 containing benzoxadiazole moieties and coumarin moieties bound via ethylenediamine have been reported for the detection of ClO^- ions [68]. Receptor has excellent selectivity and anti-interference ability toward ClO^-, and the ratio of fluorescence intensity ($I_{471\ nm}/I_{533\ nm}$) has a very good linear relationship with the concentration of ClO^-, with a wide linear range (2.5 – 1750 μM) and low detection limit (0.887 μM). The receptor have successfully applied it for the quantitative detection of ClO^- in water samples in daily life. The blue/green value (B/G) of this color change also shows a very good linear relationship to ClO^- (5.0–1000 μM). Further the receptor R48 has also been successfully used for test strip detection and quantitative detection of ClO^- in actual samples through smartphone-based fluorescence image analysis, and this method can provide faster, more convenient and more accessible detection (Fig. 54).

Aggregation Induced Emission

The primary cause of the AIE phenomenon is the restriction of intramolecular motion, rotation, or vibration (RIM, RIR, or RIV) within aggregates. AIE-active molecules exhibit weak emission in solution due to free intramolecular motions, but they become highly emissive upon aggregation in a suitable environment through the activation of RIM, RIR, or RIV mechanisms in the excited state. This unusual fluorescence behavior allows the AIE phenomenon to be effectively used in designing fluorescent probes with appropriate chelating groups for detecting metal ions. The aggregation of AIE probes can be modulated by metal ions through electrostatic interactions, coordination interactions, or the effects of polarity and viscosity (Fig. 55).

Highly fluorescent aggregation induced emission based 1, 8-naphthalimide- sulfamethizole sensor R49 have been reported for Hg^{2+} and Ag^+ ions [69]. Aggregation induced emission caused by hydrophobic nature of naphthalimide fluorogenic moiety in DMSO: water (1:99 v/v, pH 7.2, HEPES buffer). Upon the addition of various metal ions, Hg^{2+} ions shows a increases in absorbance at 267 nm and 343 nm with a slight red shift (hypochromic effect). An excimeric group obtained from the intramolecular interaction between the naphthalimide moieties in the completion of R49 with Hg^{2+} ion. Due to this reason Sensor R49 emission band at 390 nm quenched and a new intensity band appeared at 483 nm in the presence of Hg^{2+} ions. The sensor R49 -Hg^{2+} coordination restricting the free rotations of the R49 and increases the rigidity of the molecular assembly,

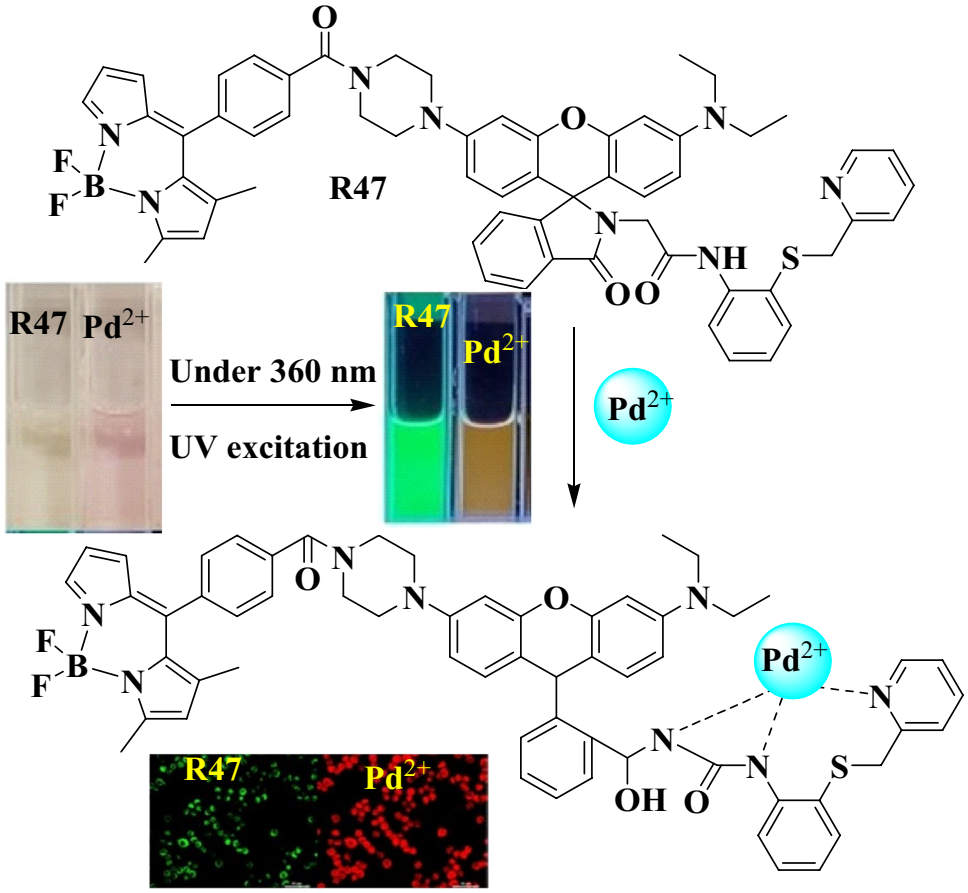

Fig. 53 Sensing mechanism of R47 towards Pd^{2+} and its fluorescence bioimaging

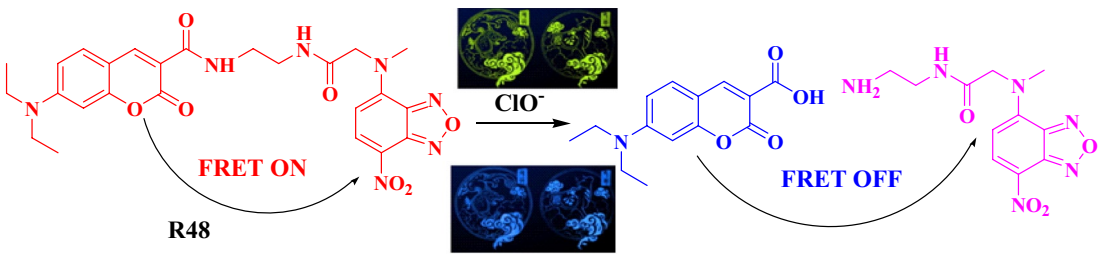

Fig. 54 Structure of R48 and its sensing mechanism with ClO^- ions

resulting a enhanced fluorescence intensity at 483 nm. Further, significantly enhancing fluorescence intensity was observed by the increasing addition of Hg^{2+} ions. Mercury ions induce more aggregation of the R49 -Hg^{2+} complex thereby facilitates the aggregation induced emission enhancement behavior of the R49. Sensor R49 sensitively detects Hg^{2+} ions and the calculated detection limit of R49-Hg^{2+} ions is 14.7 nM (Fig. 56).

A new fluorescent sensor R50a-b based on sulfonamidospirobifluorenes was synthesized and reported for the selective detection of Hg^{2+} ions in DMSO/HEPES buffer mixture [70]. Out of twenty metal ions, sensor R50a-b only shows an excellent selectivity towards Hg^{2+} ions and showed a selective fluorescence quenching (107-folds). The sulfonamide group coordinates to Hg^{2+} ions that direct to an aggregation of such complex via the face-to-face stacking of the spirobifluorene cores. At neutral pH, the sulfonamide group coordinates with Hg^{2+} ions and could promote a deprotonation of the –NH group in R50a-b. The detection limits of R50a-b with Hg^{2+} ions were found to be 10.4 nM and 103.8 nM for the derivatives bearing two and four sulfonamide groups, respectively (Fig. 57).

A chromone-based ratiometric fluorescent receptor R51 was developed for the selective detection of Hg(II) in a semi-aqueous solution based on aggregation-induced emission (AIE) and chelation-enhanced fluorescence (CHEF) effect

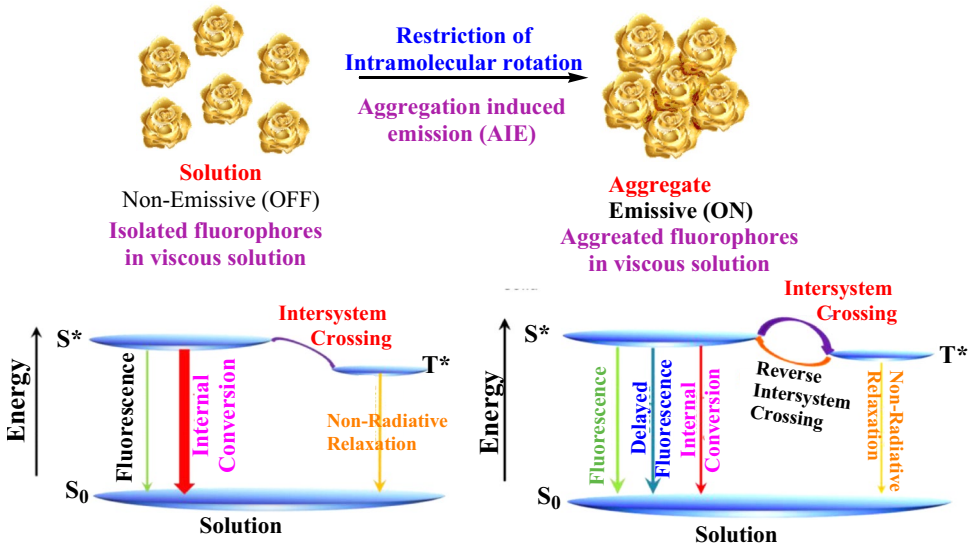

Fig. 55 Aggregation induced emission

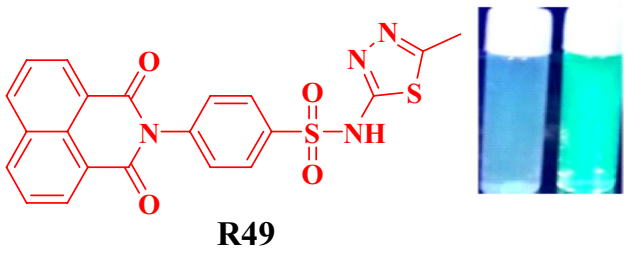

Fig. 56 Structure of R49

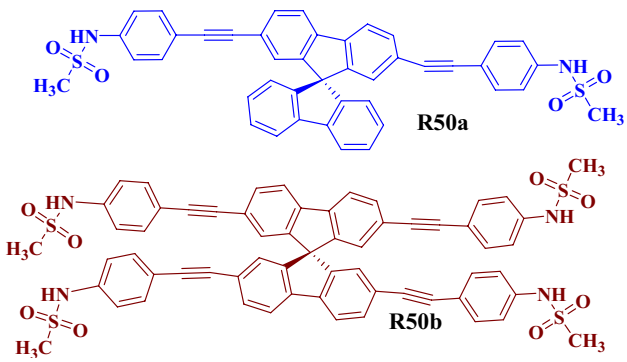

Fig. 57 Structure of R50a-b

[71]. The receptor R51 fluoresced significantly at 498 nm in its aggregated state, and when chelated with Hg^{2+}. The stoichiometry, association constant and detection limit of R51 with Hg^{2+} was found to be 1:1, 9.10×10^3 M^{-1} and 22.47 nM, respectively without interference from other interfering ions. The FTIR, ESI mass, and DFT-based computational studies investigated the binding mechanism of receptor R51 with Hg^{2+}. Taking advantage of its AIE characteristics, the receptor R51 was successfully applied for bio-capability analysis in Caenorhabditis elegans imaging of Hg^{2+} in a living model (Fig. 58).

Y. Li et al. reported [72] a novel fluorescence receptor R52 for selective and sensitive detection for Hg^{2+} and CN^- ions in DMF-H_2O (13:12, v/v). Receptor R52 shows a nonemissive spectrum in a pure organic solvent (DMF) & low concentrated aqueous system. When the water content is increased to 60%, significantly the fluorescence emission band at 650 nm increased and in 80% water the emission intensity band reached its maximum (120 fold). Slight decrease of fluorescence intensity was observed when adding further water in R52. This is due to the formation of amorphous aggregates. The emission intensity of R52 gradually inclined and reaches the maximum along with a small bathochromic shift (50 nm) upon the addition of Hg^{2+} ions. Under a UV lamp (360 nm), R52-Hg^{2+} complex results a strong red fluorescence and the calculated detection limit to be 6.6 nM. The enhancement of fluorescence is due to the aggregation induced by coordination of thymine units with Hg^{2+} ions (Fig. 59).

A novel aggregation-induced emission based receptor R53 designed [73], synthesized and reported for selective recognition of Hg^{2+} ions in a mixture of CH_3CN:H_2O (60%). Receptor R53 further used to quantitatively measure the bioaccumulation of Hg^{2+} within a small invertebrate, D. *carinata*. When excite receptor R53 at 350 nm the emission intensity increased from 0.17 to 1038.6 upon the gradual addition of Hg^{2+} ions (6100-fold). D. *carinata* alone shows no fluorescence signals and when incubated in R53 showed blue fluorescence (460–500 nm). In the presence of Hg^{2+} ions, D. *carinata*- R53 showed red fluorescence in the red channel in the 570–610 nm wavelength range. From the fluorescent microscopy studies it clearly recognizes in vivo dispersion and distribution of Hg^{2+} in D.*carinata* (Fig. 60).

Fig. 58 Structure of R51

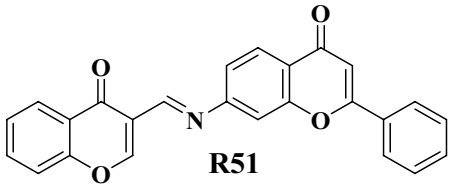

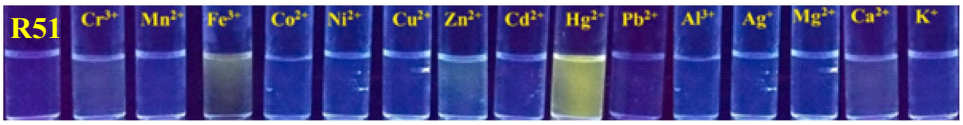

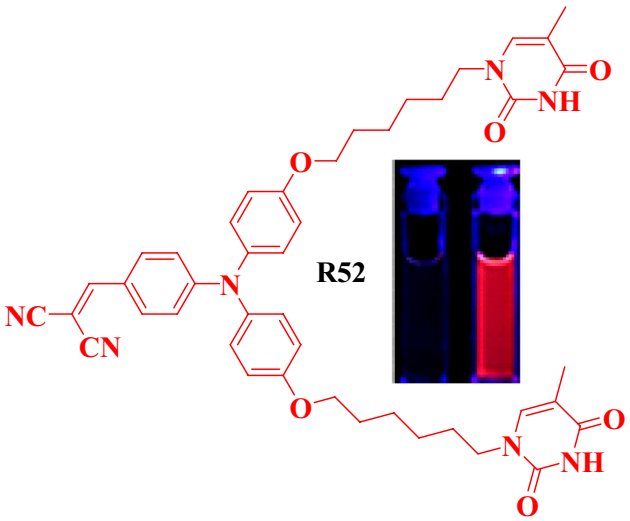

Fig. 59 Structure of R52

A novel 8-hydroxyquinoline functionalized pillar[5]arene receptor R54 was synthesised and sensor selectively recognize toxic Hg^{2+} ions selectively based on AIE fluorescence mechanism in aqueous solution [74]. Receptor R54 almost shows non fluorescence in pure organic system (DMF). Once increasing the water content, R54 displays strong fluorescence emission intensity at 410 nm (7.88-fold) due to aggregation of fluorescence. Upon the addition of various metal ions into R54, Hg^{2+} ions could significantly quench the fluorescence over other ions at 410 nm. Under the UV lamp the fluorescence color of R54 (20% H_2O) changed from blue to colorless upon the addition of Hg^{2+} ions. The detection limit of R54 towards Hg^{2+} ions was calculated to be 0.24 nM. Further based on the above results, Hg^{2+} detection test kit was prepared by using R54 sensor on a silica gel plate and the test kit could detect Hg^{2+} ions more conveniently and effectively (Fig. 61).

A series of novel pyridopyrazine derivatives based receptor R55a-d were synthesized and developed for selective and sensitive detection for Hg^{2+} ions in H_2O-CH_3CN mixture [75]. Receptor R55a showed highly twisted conformation with no π-π stacking interactions. All the receptor R55a-d are showed a weak fluorescence emission in CH_3CN solution. In higher water fractions receptor R55a-d displayed a strong enhancement of emission intensity with slight red shift in emission maxima. Pyridopyrazine derivatives of receptor R55a-d bearing electron withdrawing biphenyl rings showed "turn-on" whereas receptor R55a-d bearing electron donating biphenyl rings showed "turn-off" fluorescent response towards Hg^{2+} ions in aqueous media. The detection limits of receptor R55a-d towards Hg^{2+} were found to be in submicromolar range. The other competitive metal ions such as Na^+, K^+, Mg^{2+}, Ca^{2+}, Ba^{2+}, Cr^{3+}, Fe^{3+}, Fe^{2+}, Co^{2+}, Ni^{2+}, Cu^{2+}, Ag^+, Zn^{2+}, Cd^{2+}, Al^{3+} and Pb^{2+} didn't shows a fluorescence response with receptor R55a-d (Fig. 62).

An aggregation induced emission based receptor R56 ((E)-4-((2-hydroxy-5 methoxybenzylidene)amino)benzoic

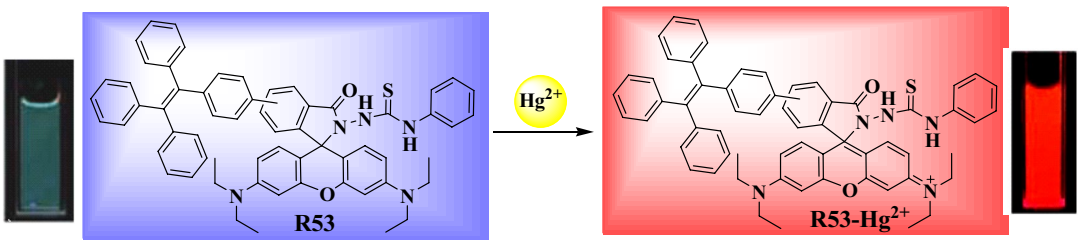

Fig. 60 Structure of R53

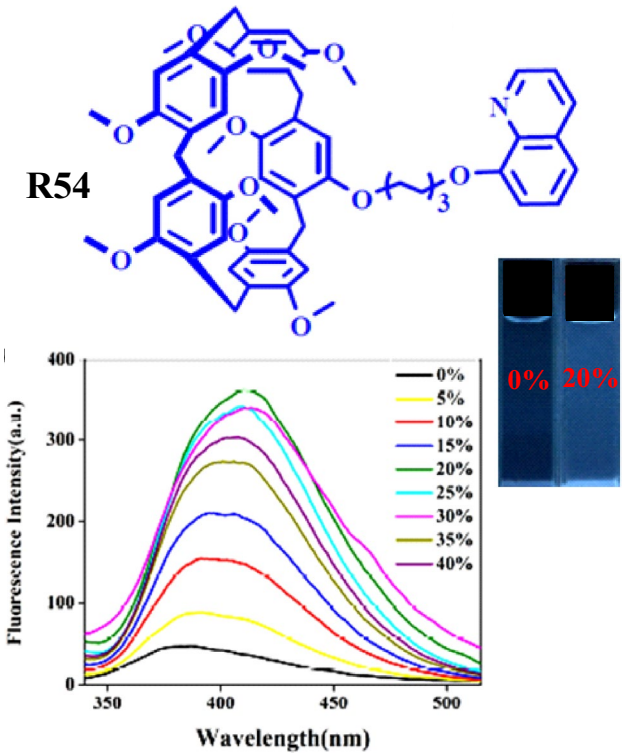

Fig. 61 Structure of R54

acid) was synthesized through facile Schiff base condensation and characterized by various spectral techniques [76]. The as-prepared compound represented a typical aggregation induced emission behavior in aqueous solution and exploited as a turn-off fluorescent sensor for Fe^{3+} detection in THF-H_2O system (3:7, v/v) with high sensitivity and selectivity. The mechanism of the fluorescence quenching was intensively studied, which was attributed to both dynamic quenching and inner filter effect. The fluorescence probe displayed a highly broad dynamic response range (0.5–500 μM) for selective detection of Fe^{3+} with a limit of detection of 0.079 μM. The proposed method was successfully employed for detection and quantification of Fe^{3+} in human urine samples and proved to have potential for practical applications in biological field (Fig. 63).

Conclusion

Fluorescent chemosensors have revolutionized the field of toxic ion detection due to their remarkable sensitivity, selectivity, and rapid response capabilities. This review has highlighted the significant advancements in the development of chemosensors based on these mechanisms, showcasing their design principles, operational mechanisms, and practical applications in detecting environmentally and biologically relevant toxic ions. Each of the five mechanistic approaches offers unique advantages and has led to the creation of highly specialized sensors. PET-based chemosensors are celebrated for their ability to detect metal ions with high sensitivity due to their electron transfer properties. FRET-based sensors excel in applications requiring conformational sensitivity and ratiometric measurements, providing reliable and precise detection of ions like Zn^{2+}, Cu^{2+} and Hg^{2+}. ICT sensors, with their wavelength-shifting capabilities, are particularly effective for detecting ions, benefiting from the significant electronic perturbations induced by ion binding. AIE sensors, exploiting the unique properties of aggregation-induced fluorescence, have opened new avenues for sensing in complex biological and environmental samples. ESIPT sensors, with their dual-emission characteristics, offer high sensitivity and ratiometric detection, making them suitable for detecting a variety of ions under diverse conditions.

Despite these advances, challenges remain in the development of fluorescent chemosensors. Issues such as background interference, sensor stability, and selectivity in complex matrices need to be addressed. Detecting toxic ions at very low concentrations, which are often found in real-world environmental and biological samples, is a significant challenge. The need for real-time, in situ monitoring of toxic ions is growing, but current technologies often lack the speed and efficiency required for such applications. Moreover, the integration of these sensors into practical devices for field use and their scalability for industrial applications require further research and innovation. The future of fluorescent chemosensors lies in addressing current limitations and expanding their applicability. Several promising avenues for future research and development include improving selectivity and sensitivity, multiplexed sensing, and exploration of new mechanisms, designing biocompatible and environmentally sustainable chemosensors. The field of fluorescent chemosensors for detecting toxic ions can be significantly extended by integrating advanced technologies such as portable sensors to develop compact, user-friendly devices for on-site detection and monitoring. Designing multifunctional chemosensors capable of detecting multiple toxic ions simultaneously will improve efficiency and reduce analysis time. The continued innovation in the design and application of fluorescent chemosensors holds great promise for the future of toxic ion detection.

Fig. 62 Structure of S55a-d

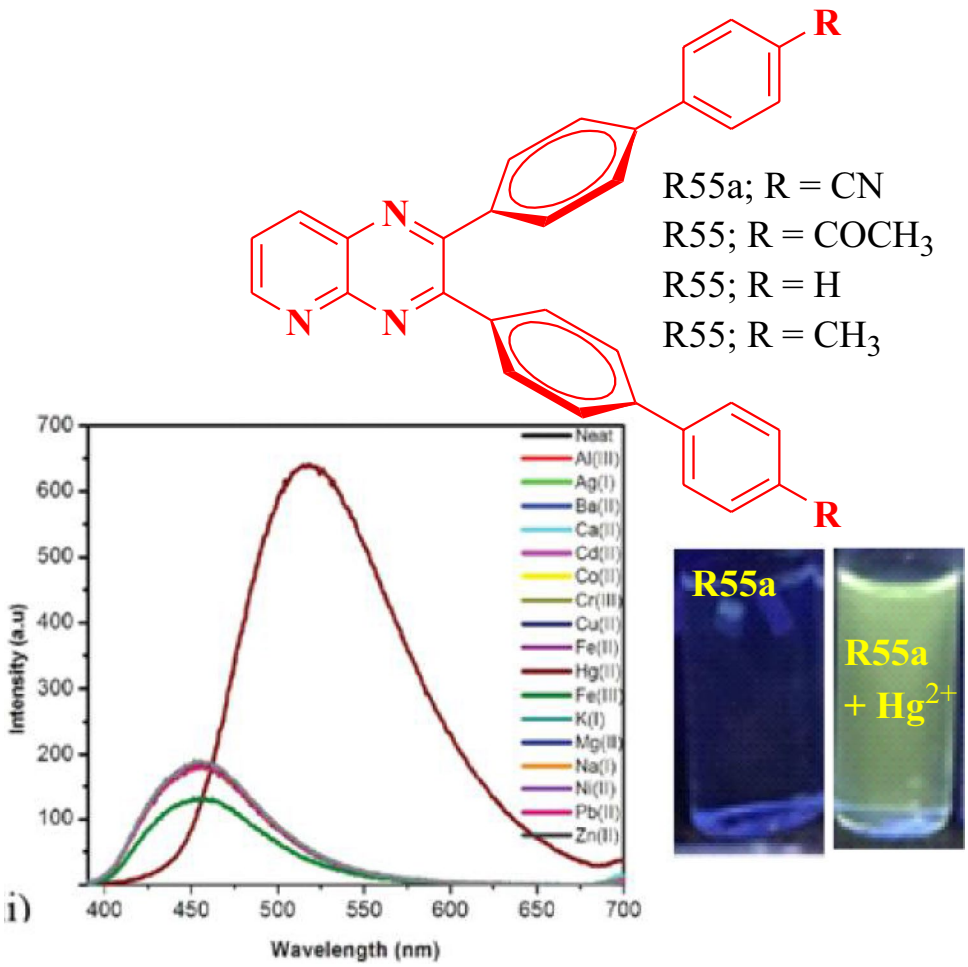

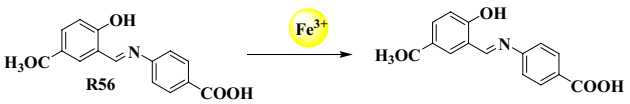

Fig. 63 Structure of R56

Table 1 Summary of mechanism based analytes detection using colorimetric and fluorescent chemosensor method

ReceptorNumber	Functional group	Method	Sensing ions	Solvent medium	Mechanism	Binding ratio	LOD	Reference No
R1	Quinoline	Fluorescence	Al^{3+}	Methanol-Aqueous	PET	1:2	1 μM	[21]
R2	Schiff base	Colorimetric & Fluorescence	Cu^{2+}	Tris–HCl buffer	ESIPT & PET	1:1	8.08 nM	[22]
R3	Benzoimidazole	Colorimetric & Fluorescence	Cu^{2+}	CH_3CN-HEPES buffer	PET	1:1	1.86	[23]
R4	Quinoline	Fluorescence	Hg^{2+}, Zn^{2+} and Cd^{2+}	$CHCl_3/CH_3OH$-H_2O	PET	1:1	-	[24]
R5	Acetamide	Fluorescence	Zn^{2+} and Cd^{2+}	Water	PET	1:1	-	[25]
R6	Quinoline	Colorimetric & Fluorescence	Zn^{2+}	EtOH-H_2O	PET	1:1	2.9 nM	[26]
R7	Schiff base	Fluorescence	Zn^{2+}	Ethanol	PET	1:1	35 μM	[27]
R8	Acetamide	Colorimetric & Fluorescence	Zn^{2+}	MeOH-Tris buffer	PET	1:1	37 μM	[28]
R9	Quinoline	Fluorescence	Zn^{2+}	HEPES buffer	PET	1:1	0.117 nM	[29]
R10	Xanthen	Fluorescence	Zn^{2+}	KOH + KCl	PET	1:1	1–5 μM	[30]
R11	Benzoimidazole	Colorimetric & Fluorescence	Zn^{2+}	CH_3OH-H_2O	PET	1:1	15 μM	[31]
R12	Quinoline	Fluorescence	Zn^{2+}	Bis–tris Buffer solution	PET	1:1	4.48 μM	[32]
R13	Quinoline	Fluorescence	Zn^{2+}	MeCN- bis–tris buffer	PET	1:1	7.1 μM	[33]
R14	Quinoline	Fluorescence	Zn^{2+} and Al^{3+}	EtOH-H_2O	ICT	1:1	3.56 μM (Zn^{2+}), 1.14 μM (Al^{3+})	[34]
R15	Acetamide	Fluorescence	Zn^{2+} and Cd^{2+}	Ethanol	PET & ICT	1:1	-	[35]
R16	Chromene	Colorimetric & Fluorescence	Zn^{2+}	CH_3CN:H_2O	ICT	1:1	48.1 nM	[36]
R17	Quinoline	Fluorescence	Zn^{2+}	CH_3CN–H_2O	ICT & CHEF	1:1	3.8 μM	[37]
R18	Schiff base	Colorimetric & Fluorescence	Zn^{2+}	THF-H_2O	ICT	1:2	-	[38]
R19	Quinoline	Fluorescence	Zn^{2+}	EtOH-H_2O	ICT & CHEF	1:1	0.024 to 0.431 μM	[39]
R20	Imidazole	Fluorescence	Zn^{2+} & Cd^{2+}	Water – DMF	ICT	1:1	-	[40]
R21	Schiff base	Fluorescence	Zn^{2+} & Hg^{2+}	DMSO–H_2O	ICT	1:1	0.011 μM & 0.040 μM	[41]
R22	Quinoline	Fluorescence	Zn^{2+}	CH_3OH-H_2O	ICT	-	-	[42]
R23	Acetamide	Fluorescence	Zn^{2+}	CH_3OH-H_2O	ICT	1:1	-	[43]
R24	Quinoline	Fluorescence	Zn^{2+}	Ethanol–Water	ICT	1:1	-	[44]
R25	Quinoline	Fluorescence	Zn^{2+}	Ethanol–Water	ICT	1:1	27 μM	[45]
R26	Schiff base	Colorimetric & Fluorescence	F^- & AcO^-	DMSO	ICT	1:1	0.67 nM (F^-) 12 μM (AcO^-)	[46]
R27	Benzothizole	Chromogenic and Fluorogenic	HOCl	DMF – PBS buffer	ESIPT	-	40 nM	[47]
R28	Flavone	Chromogenic and Fluorogenic	H_2S	Ethanol – H_2O	ESIPT	-	0.63 μM	[48]
R29	Naphthalimide	Chromogenic and Fluorogenic	Al^{3+} & F^-	CH_3CN/ H_2O	ESIPT	-	75 μM	[49]
R30	Anthraquinone	Fluorogenic	-	Acetonitrile	ESIPT	-	-	[50]

Table 1 (continued)

ReceptorNumber	Functional group	Method	Sensing ions	Solvent medium	Mechanism	Binding ratio	LOD	Reference No
R31	Schiff base	Fluorogenic	Al^{3+}	Ethanol	ESIPT	1:1	2.59 μM	[51]
R32	Schiff base	Colorimetric & Fluorogenic	Al^{3+}	DMSO-H_2O	ESIPT	1:1	82 nM	[52]
R33	Schiff base	Colorimetric & Fluorogenic	Hg^{2+} Pb^{2+}	Buffer solution	ESIPT	2:1	8.3 nM 10.5 nM	[53]
R34	Schiff base	Fluorogenic	Cu^{2+}	Ethanol-H_2O	ESIPT	-	0.08 μM	[54]
R35	Schiff base	Colorimetric & Fluorogenic	Zn^{2+}	DMSO-H_2O	ESIPT	-	0.11.nM	[55]
R36	Schiff base	Colorimetric & Fluorogenic	Cu^{2+} & F^{-}	DMSO	ESIPT	1:2	3.51 μM 3.26 μM	[56]
R37	Schiff base	Fluorogenic	F^{-}	DMSO-H_2O	ESIPT	1:1	0.12 μM	[57]
R38	Schiff base	Colorimetric & Fluorogenic	N_2H_4 CN-	DMSO-H_2O	ESIPT	1:1	1.47 μM 0.4 nM	[58]
R39	Schiff base	Fluorogenic	Al^{3+}	Methanol	ESIPT	1:1	5.48 nM	[59]
R40	Benzothiazole	Colorimetric & Fluorogenic	Fe^{3+}	CH_3OH-H_2O	FRET	1:1	0.53 nM	[60]
R41	Naphthalimide	Colorimetric & Fluorogenic	Cu^{2+}	CH_3OH-H_2O	FRET	1:1	1.50 μM	[61]
R42	Piperazin	Colorimetric & Fluorogenic	SO_3^{2-}	Ethanol – PBS	FRET	-	39 nM	[62]
R43	Naphthalimide	Fluorogenic	Hg^{2+}	-	FRET	-	30 nM	[63]
R44	Naphthalimide	Fluorogenic	Hg^{2+}	Ethanol – PBS	FRET	1:1	57 μM	[64]
R45	Rhodamine B	Colorimetric & Fluorogenic	Hg^{2+}	CH_3OH-H_2O	FRET	1:1	0.059 μM	[65]
R46	Rhodamine B	Colorimetric & Fluorogenic	Bi^{3+}	DMSO-H_2O	FRET	1:1	0.05 μM	[66]
R47	Rhodamine B	Colorimetric & Fluorogenic	Pd^{2+}	CH_3CN-H_2O	FRET	1:1	-	[67]
R48	Coumarin	Colorimetric & Fluorogenic	ClO^{-}	-	FRET	-	0.887 μM	[68]
R49	Naphthalimide	Fluorogenic	Hg^{2+}	DMSO-H_2O	AIEE	-	14.7 nM	[69]
R50	Fluorene	Fluorogenic	Hg^{2+}	DMSO-Buffer	AIEE	-	10.4 nM	[70]
R51	Chromone	Fluorogenic	Hg^{2+}	DMSO	AIEE	1:1	22.47 nM	[71]
R52	Thymine	Fluorogenic	Hg^{2+}	DMF-H_2O	AIEE	-	6.6 nM	[72]
R53	Rhodamine B	Fluorogenic	Hg^{2+}	CH_3CN-H_2O	AIEE	-	-	[73]
R54	Quinoline	Fluorogenic	Hg^{2+}	DMF	AIEE	-	0.24 nM	[74]
R55	Pyrazine	Fluorogenic	Hg^{2+}	CH_3CN-H_2O	AIEE		–	[75]
R56	Benzylidene	Fluorogenic	Fe^{3+}	THF-H_2O	AIEE	-	0.079 μM	[76]

Acknowledgements Not Applicable.

Author Contributions The sole author prepared the whole manuscript.

Funding No funding.

Data Availability No datasets were generated or analysed during the current study.

Declarations

Competing Interest The authors declare no competing interests.

References

1. Al-Saidi HM, Khan S (2024) Recent advances in thiourea based colorimetric and fluorescent chemosensors for detection of anions and neutral analytes: a review. Cri Rev Anal Chem 54:93–109. https://doi.org/10.1080/10408347.2022.2063017
2. Algethami JS, Al-Saidi HM, Alosaimi EH, Alnaam YA, Al-Ahmary KM, Khan S (2024) Recent advancements in fluorometric and colorimetric detection of Cd2+ using organic chemosensors: a review (2019–2024). Cri Rev Anal Chem 1–20:1. https://doi.org/10.1080/10408347.2024.2339968
3. Chatterjee S, Liu B, Peng H-S (2024) Chelation strategies in spiropyran-based chemosensors for colorimetric and fluorescent sensing of metal ions and anions. Coord Chem Rev 508:215779. https://doi.org/10.1016/j.ccr.2024.215779
4. Ye F-Y, Hu M, Zheng Y-S (2023) Advances and challenges of metal ions sensors based on AIE effect. Coor Chem Rev 493:215328. https://doi.org/10.1016/j.ccr.2023.215328
5. Afrin AC, Ayya Swamy P (2023) Novel Schiff base derivatives for the detection of one-to-multi metal ions and tracking the live cell imaging. Coor Chem Rev 494:215327. https://doi.org/10.1016/j.ccr.2023.215327
6. Udhayakumari D, Jerome P, Vijay N, Oh T-H (2024) ESIPT: an approach and future perspective for the detection of biologically important analytes. J Lumin 267:120350. https://doi.org/10.1016/j.jlumin.2023.120350
7. Abhijna Krishna R, Velmathi S (2024) Exploring fluorescent and colorimetric probes for analyte detection: utilizing it in live cell imaging and real-time sample analysis. Inorg Chem Acta 567:122039. https://doi.org/10.1016/j.ica.2024.122039
8. Wang J, Li Y, Patel NG, Zhang G, Zhou D, Pang Y (2014) A single molecular probe for multi-analyte (Cr^{3+}, Al^{3+} and Fe^{3+}) detection in aqueous medium and its biological application. Chem Commun 50:12258. https://doi.org/10.1039/C4CC04731A
9. Picci G, Montis R, Gilchrist AM, Gale PA, Caltagirone C (2024) Fluorescent and colorimetric sensors for anions: highlights from 2020 to 2022. Coord Chem Rev 501:215561. https://doi.org/10.1016/j.ccr.2023.215561
10. Liu S, Zhang L, Kim H, Sun J, Yoon J (2024) Recent advances and challenges in monitoring chromium ions using fluorescent probes. Coord Chem Rev 501:215575. https://doi.org/10.1016/j.ccr.2023.215575
11. David CI, Lee H (2024) Cutting-edge advances in colorimetric and fluorescent chemosensors for detecting lethal cyanide ion: a comprehensive review. Microchem J 200:1160359. https://doi.org/10.1016/j.microc.2024.110359
12. Prabakaran G, Narmatha G, Velmurugan K, Basith A, Karthick R, Velraj G, Kumar RS, Nandhakumar R (2024) Imidazole derived PET based reversible dual fluorescent chemosensor: sensing of zinc and carbonate ions and their usage on real samples and live cells. J Mol Struct 1295:136684. https://doi.org/10.1016/j.molstruc.2023.136684
13. Mohasin M, Khan SA (2024) A review on Pyrazolines as colorimetric fluorescent chemosensors for Cu^{2+}. J Fluoresc. https://doi.org/10.1007/s10895-024-03678-w
14. Sogra S, Aishwarya V, Chaithra PS, Suchi L, Abhishek S, Vishnu S, Das AK (2024) A prompt study on recent advances in the development of colorimetric and fluorescent chemosensors for "nanomolar detection" of biologically important analytes. J Fluoresc. https://doi.org/10.1007/s10895-023-03552-1
15. Chakraborty S, Das K, Halder S (2024) A review on chemo sensors and fluro sensors of mercury ions. Inorg Chimica Acta 566:122026. https://doi.org/10.1016/j.ica.2024.122026
16. Bumagina ENA, Antina V (2024) Review of advances in development of fluorescent BODIPY probes (chemosensors and chemodosimeters) for cation recognition. Coord Chem Rev 505:215688. https://doi.org/10.1016/j.ccr.2024.215688
17. Dey B, Ghosh S, Malakar CC, Atta AK (2024) Review on pyrene-based fluorometric chemosensing materials for picric acid and their AIE properties. Microchim J 200:110486. https://doi.org/10.1016/j.microc.2024.110486
18. Chakraborty S (2024) The advent of bodipy-based chemosensors for sensing fluoride ions: a literature review. J Fluoresc. https://doi.org/10.1007/s10895-024-03619-7
19. Tamrakar A, Wani MA, Mishra G, Srivastava A, Pandey R, Pandey MD (2024) Advancements in the development of fluorescent chemosensors based on C=N bond isomerization/modulation mechanistic approaches. 16: 2198–2228. https://doi.org/10.1039/D3AY02321D
20. Khan J (2024) Optical chemosensors synthesis and appplication for trace level metal ions detection in aqueous media: a review. J Fluoresc. https://doi.org/10.1007/s10895-023-03559-8
21. Jiang X-H, Wang B-D, Yang Z-Y, Liu Y-C, Li T-R, Liu Z-C (2011) 8-Hydroxyquinoline-5-carbaldehyde Schiff-base as a highly selective and sensitive Al3+ sensor in weak acid aqueous medium. Inorg Chem Commun 14:1224–1227. https://doi.org/10.1016/j.inoche.2011.04.027
22. Wang P, Fu J, Yao K, Chang Y, Xu K, Xu Y (2018) A novel quinoline-derived fluorescent "turn-on" probe for Cu^{2+} with highly selectivity and sensitivity and its application in cell imaging. Sens Actuators B: Chem 273:1070–1076. https://doi.org/10.1016/j.snb.2018.07.028
23. More PA, Shankarling GS (2017) Reversible 'turn off' fluorescence response of Cu^{2+} ions towards2-pyridyl quinoline based chemosensor with visible colour change. Sens Actuators B: Chem 241:552–559. https://doi.org/10.1016/j.snb.2016.10.121
24. Ghosh K, Tarafdar D (2013) A new quinoline-based chemosensor in ratiometric sensing of Hg^{2+} ions. Supramol Chem 25:127–132. https://doi.org/10.1080/10610278.2012.733818
25. Cai Y, Meng X, Wang A, Zhu M, Zhu Z, Guo Q-X (2013) A quinoline based fluorescent probe that can distinguish zinc(II) from cadmium(II) in water. Tetrahedron Lett 54:1125–1128. https://doi.org/10.1016/j.tetlet.2012.12.054
26. Gayathri K, Velmurugan K, Nandhakumar R, Malathi M, Mathusalini SP, Mohan S, Shankar R (2017) New pyrazoloquinoline scaffold as a reversible colorimetric fluorescent probe for selective detection of Zn^{2+} ions and its imaging in live cells. J Photochem Photobiol A Chem 341:136–145. https://doi.org/10.1016/j.jphotochem.2017.03.035
27. Fan L, Qin J-C, Li C-R, Yang Z-Y (2020) Two similar Schiff-base receptor based quinoline derivate: highly selective fluorescent probe for Zn(II). Spectrochim. Acta - A: Mol Biomol Spectrosc 236:118347. https://doi.org/10.1016/j.saa.2020.118347
28. Fu H, Liu H, Zhao L, Xiao B, Fan T, Jiang Y (2019) A quinoline-based selective 'turn on' chemosensor for zinc (II) via

quad-core complex, and its application in live cell imaging. Tetrahedron 75:130710. https://doi.org/10.1016/j.tet.2019.130710
29. Chen X-Y, Shi J, Li Y-M, Wang F-L, Wu X, Guo Q-X, Liu L (2009) Two-photon fluorescent probes of biological Zn(II) derived from 7-hydroxyquinoline. Org Lett 11:4426–4429. https://doi.org/10.1021/ol901787w
30. Nolan EM, Jaworski J, Okamoto KI, Hayashi Y, Sheng M, Lippard SJ (2005) QZ1 and QZ2: rapid, reversible quinoline-derivatized fluoresceins for sensing biological Zn(II). J Am Chem Soc 127:16812–16823. https://doi.org/10.1021/ja052184t
31. Velmurugan K, Raman A, Don D, Tang L, Easwaramoorthi S, Nandhakumar R (2015) Quinoline benzimidazole-conjugate for the highly selective detection of Zn(II) by dual colorimetric and fluorescent turn-on responses. RSC Adv 5:44463–44469. https://doi.org/10.1039/C5RA04523A
32. Choi YW, Lee JJ, Kim C (2015) A highly selective fluorescent chemosensor based on a quinoline derivative for zinc ions in pure water. RSC Adv 5:60796–60803. https://doi.org/10.1039/c5ra09954d
33. Kim YS, Lee JJ, Lee SY, Kim PG, Kim C (2016) A turn-on fluorescent chemosensor for Zn^{2+} based on quinoline in aqueous media. J Fluoresc 26:835–844. https://doi.org/10.1007/s10895-016-1771-x
34. Erdemir S, Kocyigit O, Malkondu S (2015) Fluorogenic Recognition of Zn^{2+}, Al^{3+} and F^{-} Ions by a New Multi-Analyte Chemosensor Based Bisphenol A-Quinoline. J Fluoresc 25:719–727. https://doi.org/10.1007/s10895-015-1557-6
35. Zhou X, Li P, Shi Z, Tang X, Chen C, Liu W (2012) A Highly selective fluorescent sensor for distinguishing cadmium from zinc ions based on a quinoline platform. Inorg Chem 51:9226–9231. https://doi.org/10.1021/ic300661c
36. Wu G, Gao Q, Li M, Tang X, Lai KWC, Tong Q (2018) A ratiometric probe based on coumarin-quinoline for highly selective and sensitive detection of Zn^{2+} ions in living cells. J Photochem Photobiol A Chem 355:487–495. https://doi.org/10.1016/j.jphotochem.2017.05.006
37. Praveen L, Suresh CH, Reddy MLP, Luxmi Varma R (2011) Molecular fluorescent probe for Zn^{2+} based on 2-(2-nitrostyryl)-8-methoxyquinoline. Tetrahedron Lett 52:4730–4733. https://doi.org/10.1016/j.tetlet.2011.06.099
38. Zhou X, Yu B, Guo Y, Tang X, Zhang H, Liu W (2011) Both visual and fluorescent sensor for Zn^{2+} based on quinoline platform. Inorg Chem 49:4002–4007. https://doi.org/10.1021/ic901354x
39. Vongnam K, Aree T, Sukwattanasinitt M, Rashatasakhon P (2018) Aminoquinoline-salicylaldimine dyads as highly selectiveturn-on fluorescent sensors for zinc (II) Ions. Chemistry Select 3:3495–3499. https://doi.org/10.1002/slct.201800155
40. Wang J, Lin W, Li W (2012) Single fluorescent probe displays a distinct response to Zn^{2+} and Cd^{2+}. Chem Eur J 18:13629–13632. https://doi.org/10.1002/chem.201202146
41. Dong Y, Fan R, Chen W, Wang P, Yang Y (2017) A simple quinolone schiff-base containing chef based fluorescence 'turn-on' chemosensor for distinguishing Zn^{2+} and Hg^{2+} with high sensitivity. Selectivity and Reversible Dalton Trans 46:6769–6775. https://doi.org/10.1039/C7DT00956A
42. Zhang Y, Gao X, Jia L, Xu S, Xu Z, Zhang L, Qian X (2012) Substituent-dependent fluorescent sensors for zinc ions based on carboxamidoquinoline. Dalton Trans 41:11776–11782. https://doi.org/10.1039/c2dt31139a
43. Zhang Y, Guo X, Si W, Jia L, Qian X (2008) Ratiometric and water-soluble fluorescent zinc sensor of carboxamidoquinoline with an alkoxyethylamino chain as receptor. Org Lett 10:473–476. https://doi.org/10.1021/ol702869w
44. Du J, Fan J, Peng X, Li H, Sun S (2010) The quinoline derivative of ratiometric and sensitive fluorescent zinc probe based on deprotonation. Sens Actuators B: Chem 144:337–341. https://doi.org/10.1016/j.snb.2009.09.022
45. Ma Q-J, Zhang X-B, Han Z-X, Huang B, Jiang Q, Shen G-L, Yu R-Q (2011) A ratiometric fluorescent probe for zinc ions based on the quinoline fluorophore. Int J Environ Anal Chem 91:74–86. https://doi.org/10.1080/03067310903045448
46. Yadav UN, Pant P, Sharma D, Sahoo SK, Shankarling GS (2014) Quinoline-based chemosensor for fluoride and acetate: a combined experimental and DFT study. Sens Actuators B: Chem 197:73–80. https://doi.org/10.1016/j.snb.2014.02.075
47. Jiang C, Xu X, Yao C (2022) A ratiometric fluorescence probe for imaging endoplasmic reticulum (ER) hypochlorous acid in living cells undergoing excited state intramolecular proton transfer. Spectrochim Acta - A: Mol Biomol 273:121075. https://doi.org/10.1016/j.saa.2022.121075
48. Yang L, Yang N, Gu P, Wang C, Li B, Zhang Y, Ji L, He G (2022) A novel flavone-based ESIPT ratiometric fluorescent probe for selective sensing and imaging of hydrogen polysulfides. Spectrochim Acta - A: Mol Biomol 271:120962. https://doi.org/10.1016/j.saa.2022.120962
49. Kumar G, Singh I, Goel R, Paul K, Luxami V (2021) Dual-channel ratiometric recognition of Al^{3+} and F^{-}ions through an ESIPT-ESICT signalling mechanism. Spectrochim Acta - A: Mol Biomol 247:119112. https://doi.org/10.1016/j.saa.2020.119112
50. Shang C, Wang L, Cao Y, Yu X, Li Y, Sun C, Cui J (2022) Is it possible to switch ESIPT-channel of hydroxyanthraquinones with the strategy of modifying electronic groups? J Mol Liq 347:118343. https://doi.org/10.1016/j.molliq.2021.118343
51. Kolcu F, Kaya I (2022) Carbazole-based schiff base: a sensitive fluorescent 'turn-on' chemosensor for recognition of Al(III) ions in aqueous-alcohol media. Arabian J Chem 15:103935. https://doi.org/10.1016/j.arabjc.2022.103935
52. Xu H, Chen W, Ju L, Lu H (2021) A purine based fluorescent chemosensor for the selective and sole detection of Al^{3+} and its practical applications in test strips and bio-imaging. Spectrochim Acta - A: Mol Biomol 247:119074. https://doi.org/10.1016/j.saa.2020.119074
53. Muthusamy S, Rajalakshmi K, Zhu D, Zhu W, Wang SL, Xu K-B, Zhao HL (2021) Dual detection of mercury (II) and lead (II) ions using a facile coumarin-based fluorescent probe via excited state intramolecular proton transfer and photo-induced electron transfer processes. Sens Actuators B Chem 346:130534. https://doi.org/10.1016/j.snb.2021.130534
54. Pan W, Yang X, Wang Y, Wu L, Liang N, Zhao L (2021) AIE-ESIPT based colorimetric and "OFF-ON-OFF" fluorescence Schiff base sensor for visual and fluorescent determination of Cu^{2+} in an aqueous media. J Photochem Photobiol A 420:113506. https://doi.org/10.1016/j.jphotochem.2021.113506
55. Behura R, Dash PP, Mohanty P, Behera S, Mohanty M, Dinda R, Behera S, Barick AK, Jail BR (2022) A Schiffbase luminescent chemosensor for selective detection of Zn^{2+} in aqueous medium. J Mol Struct 1264:133310. https://doi.org/10.1016/j.molstruc.2022.133310
56. Arabahmadi R (2022) Hydrazone-based Schiff base dual chemosensor for recognition of Cu^{2+} and F^{-} by 1:2 demultiplexer, half adder, half subtractor, molecular keypad lock and logically reversible transfer gate logic circuits and its application as test kit. J Photochem Photobiol A 427:113797. https://doi.org/10.1016/j.jphotochem.2022.113797
57. Karuppiah K, Nelson M, Alam MM, Selvaraj M, Sepperumal M, Ayyanar S (2022) A new 5-bromoindolehydrazone anchored diiodosalicylaldehyde derivative as efficient fluoro and chromophore for selective and sensitive detection of tryptamine and F_ ions: Applications in live cell imaging. Spectrochim Acta - A: Mol Biomol 269:120777. https://doi.org/10.1016/j.saa.2021.120777

58. Chen ZZ, Deng Y-H, Zhang T, Dong W-K (2021) A novel bifunctional-group salamo-like multi-purpose dye probe based on ESIPT and RAHB effect: distinction of cyanide and hydrazine through optical signal differential protocol. Spectrochim Acta - A: Mol Biomol 262:120084. https://doi.org/10.1016/j.saa.2021.120084
59. Akong RA, Gorls H, Woods JAO, Plass W, Eseola AO (2021) ESIPT-inspired fluorescent turn-on sensitivity towards aluminium(III) detection by derivatives of O- and S-bridged bis-(phenol-imine) molecules. Res Chem 3:100236. https://doi.org/10.1016/j.rechem.2021.100236
60. Das S, Aich K, Goswami S, Quah CK, Fun HK (2016) FRET-based fluorescence ratiometric and colorimetric sensor to discriminate Fe3+ from Fe2+. New J Chem 40:6414–6420. https://doi.org/10.1039/C5NJ03598H
61. Wang W, Mao P-D, Wu W-N, Mao X-J, Zhao X-L, Xu Z-Q, Fan Y-C, Xu Z-H (2017) A novel colorimetric, ratiometric fluorescent Cu2+ sensor based on hydrazone bearing 1, 8-naphthalimide, pyrrole moieties. Sens Actuators B Chem 251:813–820. https://doi.org/10.1016/j.snb.2017.05.134
62. Shen W, Xu H, Feng J, Sun W, Hu G, Hu Y, Yang W (2021) A ratiometric and colorimetric fluorescent probe designed based on FRET for detecting SO32-/HSO3- in living cells and mice. Spectrochim. Acta - A: Mol. Biomol. Spectrosc. 263:120183. https://doi.org/10.1016/j.saa.2021.120183
63. Zhao J, Zhang J, Hu B, Gao C, Li Z, Sun Z, You J (2023) A FRET-based ratiometric fluorescent probe for Hg2+ detection in aqueous solution and bioimaging in multiple samples. Spectrochim. Acta - A: Mol. Biomol. Spectrosc. 286:121965. https://doi.org/10.1016/j.saa.2022.121965
64. Liu J, Qian Y (2017) A novel naphthalimide-rhodamine dye: Intramolecular fluorescence resonance energy transfer & ratiometric chemodosimeter for Hg^{2+} & Fe^{3+}. Dyes Pigm 136:782–790. https://doi.org/10.1016/j.dyepig.2016.09.041
65. Xu N-Z, Liu M-M, Ye M-A, Yao Y-W, Zhou Y, Wu G-Z, Yao C (2017) A rhodamine-naphthalimide conjugated chemosensor for ratiometric detection Hg2+ in actual aqueous samples. J Lumin 188:135–140. https://doi.org/10.1016/j.jlumin.2017.03.067
66. Adhikari S, Mandal S, Ghosh A, Guria S, Pal A, Adhikary A, Das D (2018) A FRET based colorimetric and fluorescence probe for selective detection of Bi^{3+} ion and live cell imaging. J Photochem Photobiol A 360:26–33. https://doi.org/10.1016/j.jphotochem.2018.04.005
67. Tang FK, Chen Y, Nnaemaka Tritton D, Cai Z, Cham-Fai Leung K (2023) A piperazine linked rhodamine-BODIPY FRET-based fluorescent sensor for highly selective Pd2+ and biothiol detection. Chem Asian J 18:e202300477. https://doi.org/10.1002/asia.202300477
68. Ji P, Liu Y, Li W, Guo R, Xiong L, Song Z, Wang B, Feng G (2024) A new FRET-based fluorescent probe: Colorimetric and ratiometric detection of hypochlorite and anti-counterfeiting applications. Spectrochim. Acta - A: Mol. Biomol. Spectrosc. 17:124477. https://doi.org/10.1016/j.saa.2024.124477
69. Bahta M, Ahmed N (2020) An AIEE active 1, 8-naphthalimide-sulfamethizole probe for ratiometric fluorescent detection of Hg^{2+} ions in aqueous media. J Photochem Photobiol A 391:112354. https://doi.org/10.1016/j.jphotochem.2020.112354
70. Silpcharu K, Sukwattanasinitta M, Rashatasakhon P (2019) Novel sulfonamidospirobifluorenes as fluorescent sensors for mercury(II) ion and glutathione. RSC Adv 9:11451–11458. https://doi.org/10.1039/C9RA00004F
71. Ramki K, Thiruppathi G, Ramasamy SK, Sundararaj P, Sakthivel P (2024) An aggregation-induced emission-based ratiometric fluorescent chemosensor for Hg(II) and its application in Caenorhabditis elegans imaging. Methods 221:1–11. https://doi.org/10.1016/j.ymeth.2023.11.010
72. Li Y, Zhou H, Chen W, Sun G, Sun L, Su J (2016) A simple AIE-based chemosensor for highly sensitive and selective detection of Hg^{2+} and CN^{-}. Tetrahedron 72:5620–5625. https://doi.org/10.1016/j.tet.2016.07.054
73. He T, Ou W, Tang BZ, Qin J, Tang Y (2019) In vivo visualization of the process of Hg^{2+} bioaccumulation in water flea Daphnia carinata by a novel aggregation-induced emission fluorogen. Chem Asian J 14:796–801. https://doi.org/10.1002/asia.201801538
74. Ma XQ, Wang Y, Wei TB, Qi LH, Jiang XM, Ding JD, Zhu WB, Yao H, Zhang YM, Lin Q (2019) A novel AIE chemosensor based on quinoline functionalized Pillar[5]arene for highly selective and sensitive sequential detection of toxic Hg^{2+} and CN^{-}. Dyes Pigm 164:279–286. https://doi.org/10.1016/j.dyepig.2019.01.049
75. Gupta S, Milton MD (2018) Synthesis of novel AIEE active pyridopyrazines and their applications as chromogenic and fluorogenic probes for Hg^{2+} detection in aqueous media. New J Chem 42:2838–2849. https://doi.org/10.1039/C7NJ04573E
76. Li Z, Liu K, Wang Y, Han T, Han H, Zhang L, Li Y (2024) Schiff base fluorescent sensor with aggregation induced emission characteristics for the sensitive and specific Fe3+ detection. Spectrochim. Acta - A: Mol. Biomol. Spectrosc. 309:123809. https://doi.org/10.1016/j.saa.2023.123809